Quadrupolar spin liquid, octupolar Kondo coupling, and odd-frequency superconductivity in an exactly solvable model

Carlene S. de Farias,[1,2] Vanuildo S. de Carvalho,[1] Eduardo Miranda,[1] and Rodrigo G. Pereira[2]

[1]*Instituto de Física Gleb Wataghin, University of Campinas (Unicamp), Campinas, SP 13083-859, Brazil*

[2]*International Institute of Physics and Departamento de Física Teórica e Experimental, Universidade Federal do Rio Grande do Norte, Campus Universitário, Lagoa Nova, Natal, RN 59078-970, Brazil*

We propose an exactly solvable model for $j_{\text{eff}} = \frac{3}{2}$ local moments on the honeycomb lattice. Our construction is guided by a symmetry analysis and by the requirement of an exact solution in terms of a Majorana fermion representation for multipole operators. The main interaction in the model can be interpreted as a bond-dependent quadrupole-quadrupole interaction. When time reversal symmetry is explicitly broken, we obtain a gapped spin liquid with a single chiral Majorana edge mode. We also investigate another solvable model in which the time-reversal-invariant spin liquid is coupled to conduction electrons in a superconductor. In the presence of a Kondo-like coupling that involves the octupole moment of the localized spins, the itinerant electrons hybridize with the emergent Majorana fermions in the spin liquid. This leads to spontaneous time reversal symmetry breaking and generates odd-frequency pairing. Our results suggest that $j_{\text{eff}} = \frac{3}{2}$ systems with strong quadrupole-quadrupole interactions may provide a route towards non-Abelian quantum spin liquids and unconventional superconductivity.

I. INTRODUCTION

Quantum spin liquid phases have fascinated condensed matter physicists since Anderson's proposal of resonating valence bond states [1,2]. These phases harbor exotic properties such as spin fractionalization and long-range entanglement [3,4]. Unlike classical magnetic phases that spontaneously break symmetries of the Hamiltonian, quantum spin liquids are not characterized by local order parameters; in fact, their study helped develop the concept of topological order [5,6].

Kitaev's honeycomb model [7] is the best known example of an exactly solvable model with a quantum spin liquid ground state. The solution works by expressing the spin $S = \frac{1}{2}$ operators in terms of Majorana fermions and realizing that the exact excitations correspond to deconfined Majorana fermions in the background of a static $\mathbb{Z}_2$ gauge field. Experimentally, the bond-dependent anisotropic exchange interaction of the Kitaev model is realized in the iridates $(\text{Na}, \text{Li})_2\text{IrO}_3$ and the ruthenium compound α-RuCl_3 [8–10], where it is generated via the Jackeli-Khalliulin mechanism [11,12]. Essential ingredients for the latter are the strong spin-orbit coupling of $4d^5$ or $5d^5$ magnetic ions and the environment of edge-sharing octahedra formed by the ligands. The Kitaev interaction, parametrized by coupling constant K, arises as the leading term in the effective spin model for $j_{\text{eff}} = \frac{1}{2}$ local moments. A more general model that takes into account subleading exchange paths and trigonal distortions of the octahedra must also include the Heisenberg interaction J and the anisotropic interactions denoted Γ and Γ' [13,14]. As a matter of fact, the Kitaev model can be regarded as an exactly solvable point in the parameter space of the J-K-Γ-Γ' model. In the iridates and α-RuCl_3, the additional couplings beyond the Kitaev model are large enough that these materials fall outside the Kitaev

spin liquid phase and undergo magnetic ordering transitions at low temperatures [8–10].

In the past few years, alternative routes to Kitaev magnetism have been explored. In particular, the search has been extended to systems with more degrees of freedom, beyond the picture of $j_{\text{eff}} = \frac{1}{2}$ moments. For instance, materials with $4d^1$ or $5d^1$ configuration are described by effective models with $j_{\text{eff}} = \frac{3}{2}$ moments, which can be represented by pseudospin and pseudo-orbital degrees of freedom [15–18]. The higher value of j_{eff} allows for multipolar interactions which can promote hidden multipolar orders or even quantum spin-orbital liquid phases [19–23]. Multipolar interactions also play an important role in rare-earth systems [24–28], where electrons in the f shell are much more localized and have stronger spin-orbit coupling than d electrons in transition metal compounds. Indeed, rare-earth magnets analogous to $j_{\text{eff}} = \frac{1}{2}$ Kitaev materials have been proposed recently [29–31]. The spin-S Kitaev model with $S > \frac{1}{2}$, generated microscopically by Hund's coupling in the transition metal and strong spin-orbit coupling in the ligands, has also attracted considerable attention [32–37]. Unlike the original $S = \frac{1}{2}$ Kitaev model [7], however, these higher spin models are not integrable in general, and the characterization of putative quantum spin liquid phases needs to rely on numerics or analytical mean-field approximations.

In this paper, we propose an exactly solvable $j_{\text{eff}} = \frac{3}{2}$ model on the honeycomb lattice with a spin-orbital liquid ground state and Majorana fermion excitations. The guiding principles behind our construction are the exact solvability, as in previous generalizations of the Kitaev model to higher-dimensional local Hilbert spaces [38–41] and a symmetry-based analysis of the possible interactions between $j_{\text{eff}} = \frac{3}{2}$
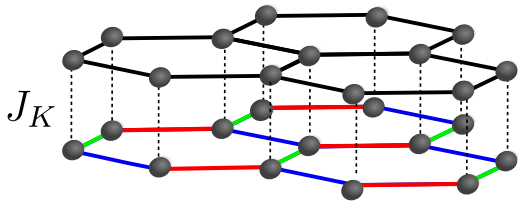
FIG. 1. Schematic representation of the honeycomb lattice containing the spin liquid (lower plane) and the itinerant electron (upper plane) degrees of freedom. The $j_{\text{eff}} = \frac{3}{2}$ local moments in the spin liquid interact via Kitaev-like quadrupole-quadrupole interactions K_γ, with $\gamma = x, y, z$ labeling the different nearest-neighbor bonds indicated by the colors red, blue, and green, respectively. The conduction electrons are described by nearest-neighbor and next-nearest-neighbor couplings which include hopping and pairing amplitudes. The two subsystems interact via a Kondo-like coupling J_K that involves the octupole moments of the localized spins.

moments in an octahedral crystal field. Whenever possible, we shall discuss the physical interpretation of the various terms in the integrable model, but here we do not attempt to derive them from detailed microscopic mechanisms for specific materials. However, our toy model can be regarded as an exactly solvable point in the parameter space of more realistic models for $j_{\text{eff}} = \frac{3}{2}$ systems. In this sense, the physical properties discussed here may be relevant to $4d^1$ or $5d^1$ materials or rare-earth systems with a Γ_8 quartet ground state [25,42] if realistic models for the latter happen to fall near the integrable point. In fact, the leading term in our Hamiltonian can be interpreted as a quadrupole-quadrupole interaction, which does appear as a symmetry-allowed term in the model for $j_{\text{eff}} = \frac{3}{2}$ honeycomb systems including the effects of Hund's coupling [21]. We also consider a single-ion anisotropy term that lowers the point group symmetry and leads to a nonzero expectation value of the local quadrupole moment, but the spin-orbital excitations remain fractionalized into Majorana fermions. Upon breaking time reversal symmetry, we obtain fully gapped spin-orbital excitations in the bulk but one gapless Majorana mode on the edge, characteristic of a non-Abelian phase with a quantized thermal Hall conductance [7].

Furthermore, we investigate the coupling of this "quadrupolar spin liquid" to itinerant electrons, as illustrated in Fig. 1. This part is motivated by recent studies of the Kondo-Kitaev model within mean-field approximations [43,44] and by *ab initio* calculations of α-RuCl$_3$/graphene heterostructures [45], which suggest that the Kondo coupling between a Fermi liquid and a Kitaev spin liquid can give rise to exotic superconductivity. Again we choose the interactions so that the total Hamiltonian is exactly solvable in terms of free Majorana fermions and conserved $\mathbb{Z}_2$ bond variables. This requires the decoupled electronic system to be a superconductor that breaks inversion and SU(2) spin rotational symmetry but preserves time reversal symmetry. The itinerant electrons and $j_{\text{eff}} = \frac{3}{2}$ local moments interact via an octupolar Kondo coupling, analogous to the coupling studied in the context of heavy-fermion systems where the magnetic ions form non-Kramers doublets [46,47]. We find that the hybridization between Majorana fermions in the spin liquid and in the superconductor leads to *spontaneous*

breaking of time reversal symmetry. Within the exactly solvable model, the ground state is degenerate between the choices of uniform ("ferro") or staggered ("antiferro") hybridization order parameters. In both cases, the effective action for the electrons in the superconductor contains odd-frequency pairing [48–55]. We then analyze the effects of weak integrability-breaking perturbations that lift this degeneracy and obtain either a gapped superconductor with chiral edge states or a gapless superconductor with a Bogoliubov Fermi surface [56] and antichiral edge states [57].

The paper is organized as follows. First, in Sec. II, we introduce the exactly solvable model with quadrupole-quadrupole interactions between local moments. In Sec. III, we consider the full model with the Kondo-like coupling between the spin liquid and the superconductor. We discuss properties of the spectrum and the spontaneous time reversal symmetry breaking in the coupled system. In Sec. IV, we calculate the effective action for the electrons in the superconductor after exactly integrating out the Majorana fermions associated with the local moments. In Sec. V, we analyze the effects of perturbations to the exactly solvable model. Finally, we present our conclusions in Sec. VI.

II. EXACTLY SOLVABLE QUADRUPOLAR SPIN LIQUID MODEL

A. Symmetry considerations

Consider local moments with effective total angular momentum $j_{\text{eff}} = \frac{3}{2}$. For concreteness, we can think of transition metal ions with a $4d^1$ or $5d^1$ configuration subject to a strong crystal field of ligand octahedra and to strong spin-orbit coupling. In this case, the single electron in the open d shell occupies the threefold degenerate t_{2g} orbitals with effective orbital angular momentum $l_{\text{eff}} = 1$. The spin-orbit coupling splits the energy levels into a higher-energy $j_{\text{eff}} = \frac{1}{2}$ doublet and the low-lying $j_{\text{eff}} = \frac{3}{2}$ quadruplet [9]. Alternatively, we may consider rare earth ions which have a quartet ground state in an octahedral crystal field [25,26].

The local Hilbert space is spanned by the four eigenstates of the J^z operator, $J^z |m_J\rangle = m_J |m_J\rangle$, with $m_J = \pm \frac{1}{2}, \pm \frac{3}{2}$. These states transform under rotations as the Γ_8 representation of the octahedral double group [42]. The operators acting in the local Hilbert space can be organized into dipole, quadrupole, and octupole moments [25,27] as shown in Table I. While the dipole and octupole moments involve odd powers of components of **J** and change sign under time reversal, the quadrupole moments contain even powers and are time-reversal invariant.

We rewrite the eigenstates of J^z in terms of two pseudospin-1/2 quantum numbers in the form $|s^z, \tau^z\rangle$ [16,25], identifying

$$
\begin{aligned}
\left| m_J = \tfrac{3}{2} \right\rangle &= \left| s^z = -\tfrac{1}{2}, \tau^z = \tfrac{1}{2} \right\rangle \equiv \left| -+ \right\rangle, \\
\left| m_J = \tfrac{1}{2} \right\rangle &= -\left| s^z = \tfrac{1}{2}, \tau^z = -\tfrac{1}{2} \right\rangle \equiv -\left| +- \right\rangle, \\
\left| m_J = -\tfrac{1}{2} \right\rangle &= \left| s^z = -\tfrac{1}{2}, \tau^z = -\tfrac{1}{2} \right\rangle \equiv \left| -- \right\rangle, \\
\left| m_J = -\tfrac{3}{2} \right\rangle &= -\left| s^z = \tfrac{1}{2}, \tau^z = \tfrac{1}{2} \right\rangle \equiv -\left| ++ \right\rangle. \quad (1)
\end{aligned}
$$

TABLE I. Local operators acting on $j_{\text{eff}} = \frac{3}{2}$ states. Overlines indicate the symmetrization with respect to permutations of the indices, e.g., $\overline{J^x(J^y)^2} = J^x(J^y)^2 + J^yJ^xJ^y + (J^y)^2J^x$. Here $\mathbf{u}^\gamma$ and $\mathbf{v}^\gamma$ are unit vectors in the xz plane given by $\mathbf{u}^x = -\frac{1}{2}\hat{\mathbf{z}} + \frac{\sqrt{3}}{2}\hat{\mathbf{x}}$, $\mathbf{u}^y = -\frac{1}{2}\hat{\mathbf{z}} - \frac{\sqrt{3}}{2}\hat{\mathbf{x}}$, $\mathbf{u}^z = \hat{\mathbf{z}}$, $\mathbf{v}^x = -\frac{\sqrt{3}}{2}\hat{\mathbf{z}} - \frac{1}{2}\hat{\mathbf{x}}$, $\mathbf{v}^y = \frac{\sqrt{3}}{2}\hat{\mathbf{z}} - \frac{1}{2}\hat{\mathbf{x}}$, $\mathbf{v}^z = \hat{\mathbf{x}}$. Adapted from Refs. [17,25].

Moment	Symmetry	Operators	$\mathbf{s}, \boldsymbol{\tau}$ representation	Majorana representation
Dipole	Γ_4	J^x	$-s^x(1 + 4\mathbf{u}^x \cdot \boldsymbol{\tau})$	$\frac{i}{2}\eta^y\eta^z - 2i\eta^x\left(-\frac{1}{2}\theta^z + \frac{\sqrt{3}}{2}\theta^x\right)$
		J^y	$-s^y(1 + 4\mathbf{u}^y \cdot \boldsymbol{\tau})$	$\frac{i}{2}\eta^z\eta^x - 2i\eta^y\left(-\frac{1}{2}\theta^z - \frac{\sqrt{3}}{2}\theta^x\right)$
		J^z	$-s^z(1 + 4\mathbf{u}^z \cdot \boldsymbol{\tau})$	$\frac{i}{2}\eta^x\eta^y - 2i\eta^z\theta^z$
Quadrupole	Γ_3	$O^{3z^2-r^2} = \frac{1}{3}[3(J^z)^2 - \mathbf{J}^2]$	$2\tau^z$	$-i\theta^x\theta^y$
		$O^{x^2-y^2} = \frac{1}{\sqrt{3}}[(J^x)^2 - (J^y)^2]$	$2\tau^x$	$-i\theta^y\theta^z$
	Γ_5	$O^{xy} = \frac{1}{\sqrt{3}}\overline{J^xJ^y}$	$-4s^z\tau^y$	$i\eta^z\theta^y$
		$O^{yz} = \frac{1}{\sqrt{3}}\overline{J^yJ^z}$	$-4s^x\tau^y$	$i\eta^x\theta^y$
		$O^{zx} = \frac{1}{\sqrt{3}}\overline{J^xJ^z}$	$-4s^y\tau^y$	$i\eta^y\theta^y$
Octupole	Γ_2	$T^{xyz} = \frac{2}{3\sqrt{3}}\overline{J^xJ^yJ^z}$	$2\tau^y$	$-i\theta^z\theta^x$
	Γ_4	$\frac{2}{3}(J^x)^3 - \frac{1}{3}(\overline{J^x(J^y)^2} + \overline{(J^z)^2J^x})$	$-2s^x(1 - \mathbf{u}^x \cdot \boldsymbol{\tau})$	$i\eta^y\eta^z + \frac{i}{2}\eta^x\left(-\frac{1}{2}\theta^z + \frac{\sqrt{3}}{2}\theta^x\right)$
		$\frac{2}{3}(J^y)^3 - \frac{1}{3}(\overline{J^y(J^z)^2} + \overline{(J^x)^2J^y})$	$-2s^y(1 - \mathbf{u}^y \cdot \boldsymbol{\tau})$	$i\eta^z\eta^x + \frac{i}{2}\eta^y\left(-\frac{1}{2}\theta^z - \frac{\sqrt{3}}{2}\theta^x\right)$
		$\frac{2}{3}(J^z)^3 - \frac{1}{3}(\overline{J^z(J^x)^2} + \overline{(J^y)^2J^z})$	$-2s^z(1 - \mathbf{u}^z \cdot \boldsymbol{\tau})$	$i\eta^x\eta^y + \frac{i}{2}\eta^z\theta^z$
	Γ_5	$\frac{2}{3\sqrt{3}}[\overline{J^x(J^y)^2} - \overline{(J^z)^2J^x}]$	$-4s^x\mathbf{v}^x \cdot \boldsymbol{\tau}$	$-i\eta^x\left(-\frac{1}{2}\theta^x - \frac{\sqrt{3}}{2}\theta^z\right)$
		$\frac{2}{3\sqrt{3}}[\overline{J^y(J^z)^2} - \overline{(J^x)^2J^y}]$	$-4s^y\mathbf{v}^y \cdot \boldsymbol{\tau}$	$-i\eta^y\left(-\frac{1}{2}\theta^x + \frac{\sqrt{3}}{2}\theta^z\right)$
		$\frac{2}{3\sqrt{3}}[\overline{J^z(J^x)^2} - \overline{(J^y)^2J^z}]$	$-4s^z\mathbf{v}^z \cdot \boldsymbol{\tau}$	$-i\eta^z\theta^x$

We refer to s^z and τ^z as the pseudospin and pseudo-orbital quantum numbers, respectively. The operators $\mathbf{s}$ and $\boldsymbol{\tau}$ acting on the corresponding degrees of freedom obey the algebra $[s^\alpha, s^\beta] = i\epsilon^{\alpha\beta\gamma}s^\gamma$, $[\tau^\alpha, \tau^\beta] = i\epsilon^{\alpha\beta\gamma}\tau^\gamma$, and $[s^\alpha, \tau^\beta] = 0$. In this notation, the time reversal operator is written as $T = -2is^y\mathcal{K}$, where $\mathcal{K}$ denotes complex conjugation. Thus, two states with the same τ^z eigenvalue form a Kramers pair. States in a non-Kramers pair, having the same s^z but different τ^z, are associated with different electronic density profiles [17]. The pseudospin and pseudo-orbital operators transform under time reversal as follows:

$$T(s^x, s^y, s^z)T^{-1} = (-s^x, -s^y, -s^z),$$
$$T(\tau^x, \tau^y, \tau^z)T^{-1} = (\tau^x, -\tau^y, \tau^z). \quad (2)$$

The representation of the multipole operators in terms of $\mathbf{s}$ and $\boldsymbol{\tau}$ is shown in Table I. We note in particular the transformation of $\mathbf{s}$ and $\boldsymbol{\tau}$ under a C_3 rotation around the [111] axis:

$$C_3(s^x, s^y, s^z)C_3^{-1} = (s^y, s^z, s^x),$$
$$C_3(\tau^x, \tau^z)C_3^{-1} = \left(\frac{-\tau^x - \sqrt{3}\tau^z}{2}, \frac{-\tau^z + \sqrt{3}\tau^x}{2}\right),$$
$$C_3\tau^yC_3^{-1} = \tau^y. \quad (3)$$

Importantly, the τ^y operator is invariant under all rotations of the octahedral group, but changes sign under time reversal. It corresponds to the octupole moment $T^{xyz} \propto \overline{J^xJ^yJ^z}$, where the overline indicates a sum over permutations of the indices, see Table I. By contrast, τ^x and τ^z are associated with quadrupole moments, and C_3 rotations act as $120°$ rotations of (τ^z, τ^x), in analogy with quantum compass models [58].

B. Time-reversal-invariant spin model

We begin with the model

$$H_s = \sum_{\gamma=x,y,z} \sum_{\langle ij\rangle_\gamma} K_\gamma O_i^{\alpha\beta}O_j^{\alpha\beta} - \lambda\sum_j O_j^{3z^2-r^2}, \quad (4)$$

where $\langle ij\rangle_\gamma$ labels a nearest-neighbor bond along the γ direction, see Fig. 1, and $O_j^{3z^2-r^2}$ and $O_j^{\alpha\beta}$ [with (α, β, γ) a cyclic permutation of (x, y, z)] are quadrupole operators defined in Table I. The first term amounts to a quadrupole-quadrupole interaction often invoked in models for f-electron systems, where it stems from electrostatic or phonon-mediated interactions [24,25,42,59]. In $4d^1/5d^1$ systems, this interaction can also be generated by the coupling $(L_i^\alpha L_i^\beta + L_i^\beta L_i^\alpha)(L_j^\alpha L_j^\beta + L_j^\beta L_j^\alpha)$ [60], where $\mathbf{L}_i$ is the $l_{\text{eff}} = 1$ orbital angular momentum operator of the t_{2g} states, upon projection onto the $j_{\text{eff}} = \frac{3}{2}$ multiplet. In fact, the isotropic quadrupole-quadrupole interaction, with $K_x = K_y = K_z$, appears in the effective spin model for $j_{\text{eff}} = \frac{3}{2}$ systems on tricoordinated lattices with edge-sharing octahedra [21]. The λ term in Eq. (4) breaks the C_3 rotational symmetry even in the isotropic case. This single-ion anisotropy term can be associated with a distortion of the local octahedral environment, which lifts the degeneracy between non-Kramers pairs [15].

To see why model (4) is exactly solvable, we introduce a Majorana fermion representation for spin 3/2 [19,38]. In terms of pseudospin and pseudo-orbital operators, we write

$$s_j^\gamma = -\frac{i}{4}\epsilon^{\alpha\beta\gamma}\eta_j^\alpha\eta_j^\beta,$$
$$\tau_j^\gamma = -\frac{i}{4}\epsilon^{\alpha\beta\gamma}\theta_j^\alpha\theta_j^\beta, \quad (5)$$

where η_j^α and θ_j^α are Majorana fermion operators that satisfy the anticommutation relations $\{\eta_j^\alpha, \eta_l^\beta\} = \{\theta_j^\alpha, \theta_l^\beta\} = 2\delta_{jl}\delta^{\alpha\beta}$ and $\{\eta_j^\alpha, \theta_l^\beta\} = 0$. Similarly to the original spin-1/2 Kitaev model [7], this Majorana fermion representation brings about a $\mathbb{Z}_2$ gauge structure, since physical observables are invariant under $(\eta_j^\alpha, \theta_j^\alpha) \mapsto (-\eta_j^\alpha, -\theta_j^\alpha)$. This gauge redundancy enlarges the Hilbert space. To restrict states to the physical Hilbert space, we must impose the local constraint

$$D_j \equiv i\eta_j^x\eta_j^y\eta_j^z\theta_j^x\theta_j^y\theta_j^z = 1 \quad \forall j. \tag{6}$$

This can be implemented to all lattice sites by the projection operator $\mathcal{P} \equiv \prod_j[(D_j + 1)/2]$. The physical states $|\psi_{\text{phys}}\rangle$ of the quadrupolar spin liquid is obtained as $|\psi_{\text{phys}}\rangle = \mathcal{P}|\psi_0\rangle$, where $|\psi_0\rangle$ denotes the wave function of the Majorana fermions. The multipole operators are rewritten in terms of Majorana fermions as given in Table I. In this representation, time reversal symmetry is implemented as complex conjugation, $TiT^{-1} = -i$, combined with

$$T\theta_j^y T^{-1} = -\theta_j^y, \tag{7}$$

leaving the other Majorana fermions invariant; see Appendix A. The C_3 rotation acts as a cyclic permutation of (η^x, η^y, η^z) and as a $120°$ rotation $(\theta^z, \theta^x) \mapsto (-\frac{1}{2}\theta^z + \frac{\sqrt{3}}{2}\theta^x, -\frac{1}{2}\theta^x - \frac{\sqrt{3}}{2}\theta^z)$, analogous to Eq. (3). Essentially, the "scalar" Majorana fermion θ^y inherits the symmetry properties of the τ^y operator.

We rewrite the Hamiltonian Eq. (4) in terms of Majorana fermions according to Table I and obtain

$$H_s = i\sum_\gamma\sum_{\langle jl\rangle_\gamma} K_\gamma \hat{u}_{\langle jl\rangle_\gamma}\theta_j^y\theta_l^y + i\lambda\sum_j\theta_j^x\theta_j^y, \tag{8}$$

where $\hat{u}_{\langle jl\rangle_\gamma} = -i\eta_j^\gamma\eta_l^\gamma$ are antisymmetric $\mathbb{Z}_2$ bond operators, obeying $(\hat{u}_{\langle jl\rangle_\gamma})^2 = 1$ and $\hat{u}_{\langle jl\rangle_\gamma} = -\hat{u}_{\langle lj\rangle_\gamma}$, which commute with one another and with H_s. Once we fix the values of the conserved $\hat{u}_{\langle jl\rangle_\gamma} = \pm1$, the Hamiltonian becomes quadratic in the remaining Majorana fermions. The ground state is in the sector with zero $\mathbb{Z}_2$ flux [61], defined as the product of $\hat{u}_{\langle jl\rangle_\gamma}$ around each hexagon. We then set $\hat{u}_{\langle jl\rangle_\gamma} = 1$ for all sites j in sublattice A and l the corresponding nearest neighbors in sublattice B. We have verified using exact diagonalization for small cluster systems that this condition gives the exact ground state energy of H_s. The resulting Hamiltonian for θ^x and θ^y is translationally invariant and can be diagonalized by a Fourier transform. Here we use the notation $\theta_j^\gamma \equiv \theta_b^\gamma(\mathbf{R})$, where $\mathbf{R}$ is the position of the unit cell and $b \in \{A, B\}$ is a sublattice index. We can then write

$$\theta_j^\gamma = \sqrt{\frac{2}{N}}\sum_{\mathbf{k}\in\frac{1}{2}\text{BZ}}[e^{i\mathbf{k}\cdot\mathbf{R}}\theta_b^\gamma(\mathbf{k}) + e^{-i\mathbf{k}\cdot\mathbf{R}}\theta_b^\gamma(-\mathbf{k})], \tag{9}$$

where the fermion operators in momentum space obey $\theta_b^\gamma(-\mathbf{k}) = [\theta_b^\gamma(\mathbf{k})]^\dagger$, and the summation runs over half of the Brillouin zone. We find the dispersion relations

$$E_s(\mathbf{k}) = \pm\frac{1}{\sqrt{2}}\sqrt{|g(\mathbf{k})|^2 + 2\lambda^2 \pm |g(\mathbf{k})|\sqrt{|g(\mathbf{k})|^2 + 4\lambda^2}}, \tag{10}$$
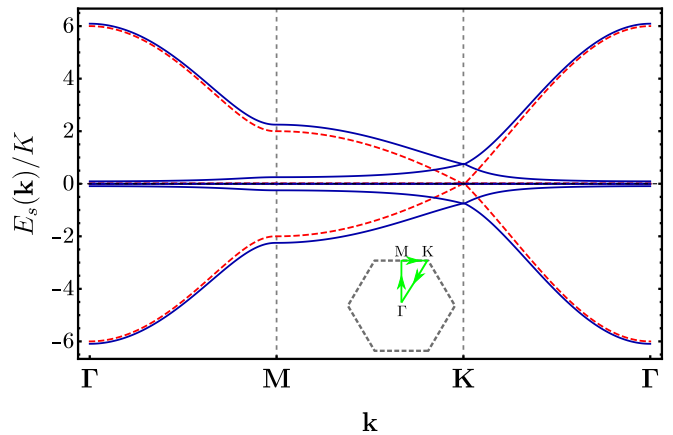

FIG. 2. Dispersion relation of the θ Majorana fermions in the quadrupolar spin liquid along the high symmetry directions on the first Brillouin zone. Here we consider isotropic interactions, $K_\gamma = K$, and two values of the single-ion anisotropy parameter: $\lambda = 0$ (dashed line) and $\lambda/K = 0.75$ (solid line).

where $g(\mathbf{k}) = K_x e^{i\mathbf{k}\cdot\mathbf{n}_1} + K_y e^{i\mathbf{k}\cdot\mathbf{n}_2} + K_z$. Here, $\mathbf{n}_1 = \frac{\sqrt{3}a}{2}(1, \sqrt{3})$ and $\mathbf{n}_2 = \frac{\sqrt{3}a}{2}(-1, \sqrt{3})$ are the primitive lattice vectors in the xy plane and we set $a = 1$.

Having been absorbed into the bond operators, the η^γ Majorana fermions are gapped out since it costs a finite energy to create $\mathbb{Z}_2$ vortices [7]. Figure 2 shows the dispersion relations for θ fermions given by Eq. (10). Hereafter we focus on isotropic interactions, $K_\gamma = K$. Note that for $\lambda = 0$ we have two flavors of Majorana fermions, θ^x and θ^z, which do not appear in the Hamiltonian. In terms of τ operators, we have a local U(1) symmetry, $[\tau_j^y, H_s] = 0$ for $\lambda = 0$. In this case, the θ^y mode displays a gapless Dirac dispersion at the K point of the Brillouin zone, whereas θ^x and θ^z modes give rise to zero energy flat bands, see Fig. 2. At each site, θ_j^x and θ_j^z can be combined into a single complex fermion which commutes with H_s, which implies that the ground state degeneracy increases exponentially with system size.

For $\lambda \neq 0$, an energy gap opens up for the modes coming from the hybridization of θ^x and θ^y, see Fig. 2. The anisotropy associated with λ lowers the ground state energy and gaps out the excitations created by the pseudo-orbital operator τ. However, the θ^z Majorana fermions still commutes with H_s. As a consequence, the ground state of the quadrupolar spin liquid is highly degenerate even for $\lambda \neq 0$. The relation between the local conservation laws and the ground state degeneracy is discussed in more detail in Appendix B. In Sec. III we will couple the Hamiltonian in Eq. (4) to conduction electrons in a superconductor. We shall see that this coupling generates a dispersion for all modes and removes the exponential degeneracy in the ground state of the total system. Alternatively, we can obtain an exactly solvable spin model with a unique ground state by breaking time reversal symmetry, as we shall discuss in the next subsection.

C. Breaking time reversal symmetry

In analogy with the Kitaev model in the presence of a magnetic field [7], we now investigate the effects of time

reversal symmetry breaking in the quadrupolar spin liquid. We break time reversal while preserving the integrability of the model by adding to the Hamiltonian in Eq. (4) the following interactions:

$$\delta H_s = \kappa \sum_{\langle ij \rangle_\alpha \langle jk \rangle_\beta} O_i^{\beta\gamma} s_j^\gamma O_k^{\alpha\gamma} - \kappa' \sum_j T_j^{xyz}. \qquad (11)$$

We propose the two terms in δH_s based only on symmetry and exact solvability, but it is worth noting that they could in principle arise as effective interactions generated by perturbation theory in a combination of a magnetic field, which couples to the time-reversal-odd pseudospin s^γ contained in the dipole operator J^γ, and strain fields which couple to the quadrupole operators $O^{\alpha\beta}$. The small parameter in this case is the ratio of the fields to the energy gap for changing the flux configuration by creating $\mathbb{Z}_2$ vortices. Using the Majorana fermion representation, we obtain

$$\delta H_s = i\kappa \sum_{\langle ij \rangle_\alpha \langle jk \rangle_\beta} \hat{u}_{\langle ij \rangle_\alpha} \hat{u}_{\langle jk \rangle_\beta} \theta_i^y \theta_k^y + i\kappa' \sum_j \theta_j^z \theta_j^x. \qquad (12)$$

We can then fix the values of the bond variables as discussed in Sec. II B and obtain a quadratic Hamiltonian $H_s + \delta H_s$ which involves all three θ^γ Majorana fermions. We assume here that both κ and κ' are much smaller than the other energy scales of the model, in order to not change the ground-state configuration of the bond variables.

In particular, for the isotropic case $\lambda = 0$, the Majorana fermions θ^x and θ^z are decoupled from θ^y. The ground state in this case is an eigenstate of the local pseudo-orbital operators τ_j^y with eigenvalue $\tau_j^y = \frac{1}{2}$ for $\kappa' > 0$. The κ term gaps out the dispersion of the θ^y Majorana fermions. Similarly to the Kitaev model [7], we expect this gapped spin liquid to be a topological phase. In fact, we find that the Chern number in this situation evaluates to $C = \pm 1$. We also obtain that, out of the three occupied bands of the θ^y Majorana fermions, only the one in the bottom of the spectrum contributes to C. To check this, we compute the energy spectrum of the model on a strip geometry with open boundary conditions in the y direction. In Fig. 3, we see that the spectrum contains one chiral Majorana edge mode, equivalent to a topological superconductor with Chern number $C = \pm 1$. This result is consistent with a recent conjecture for spin-S Kitaev spin liquids [37], which states that when time-reversal symmetry is broken Kitaev spin liquids with half-integer spin S exhibit a non-Abelian phase, while those with integer S possess, in contrast, an Abelian one. Our $j_{\text{eff}} = \frac{3}{2}$ model is analogous to the $S = \frac{3}{2}$ Kitaev model in the sense of a four-dimensional local Hilbert space, and indeed we find that the Chern number is odd, corresponding to a non-Abelian phase with quantized thermal Hall conductance $\kappa_{xy}/T = \pi/12$ [7].

We also note that for $\lambda \neq 0$ the eigenstates of the Hamiltonian are no longer eigenstates of τ_j^y. In this case, the coupling of $\theta^{x,z}$ to θ^y turns the dispersionless modes seen in Fig. 3(a) into a band of mobile pseudo-orbital excitations as shown in Fig. 3(b). As expected, we also find $C = \pm 1$ for the Chern number. In contrast with the $\lambda = 0$ behavior, all occupied bands acquire here a nontrivial band topology, contributing with ± 1 to this value of the Chern number.
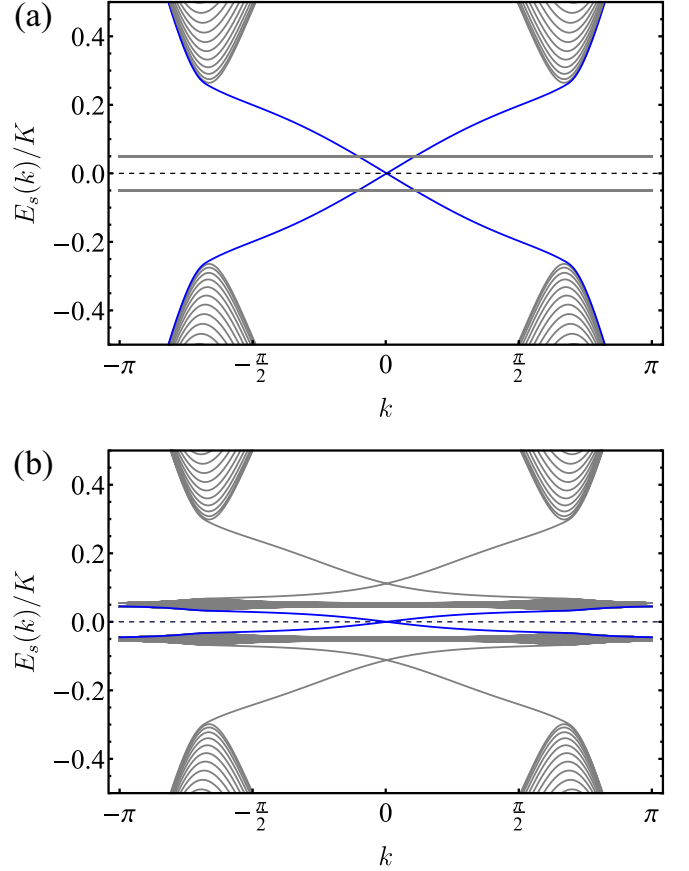

FIG. 3. Band structure of the gapped spin liquid with broken time reversal symmetry on a strip with zigzag edges and width $W = 80$ unit cells. Here we set $\kappa = \kappa' = 0.05K$ and consider two values of λ: (a) $\lambda = 0$; (b) $\lambda = 0.1K$. In both cases, the dispersion of the edge mode crosses zero energy at a single point in the projection of the Brillouin zone.

III. COUPLING THE SPIN LIQUID TO A SUPERCONDUCTOR

We now turn to the Hamiltonian

$$H = H_s + H_c + H_K. \qquad (13)$$

Here, H_s describes the quadrupolar spin liquid in Eq. (4), and we shall assume $\lambda \neq 0$. The new terms, H_c and H_K, describe, respectively, the conduction electrons in the superconductor and the Kondo coupling between electrons and $j_{\text{eff}} = \frac{3}{2}$ local moments. Our goal in this section is to write down H_c and H_K that produce an exactly solvable model without any zero-energy flat bands. We shall see that the Kondo coupling gives rise to time-reversal-symmetry-breaking superconductivity.

A. Time-reversal-invariant superconductor

The following Bogoliubov-de-Gennes Hamiltonian describes the itinerant electron system:

$$H_c = i \sum_{\langle jl \rangle} \Psi_j^\dagger [t_{jl}(\sigma^x \rho^z + \sigma^z \rho^x) + w_{jl}(\sigma^z \rho^z - \sigma^x \rho^x)]\Psi_l$$
$$+ i \sum_{\langle\langle jl \rangle\rangle} t'_{jl} \Psi_j^\dagger (\sigma^x \rho^z + \sigma^z \rho^x)\Psi_l. \qquad (14)$$
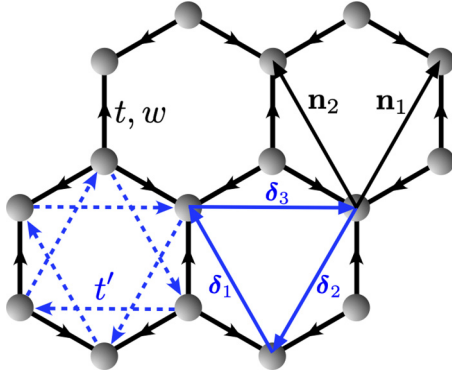
FIG. 4. Couplings in the Hamiltonian for itinerant electrons. Nearest-neighbor bonds with couplings t and w are oriented from the A to the B sublattice. Next-nearest-neighbor bonds with coupling t' are oriented as indicated by the blue dashed arrows.

The operator Ψ_j refers to the Balian-Werthamer spinor of the conduction electrons:

$$\Psi_j = \begin{pmatrix} \psi_j \\ -i\sigma^y (\psi_j^\dagger)^T \end{pmatrix}, \tag{15}$$

where $\psi_j = (\psi_{j\uparrow}, \psi_{j\downarrow})^T$. The Pauli matrices σ^α and ρ^α act in spin space and Nambu space, respectively. The parameters $t_{jl} = -t_{lj}$, $w_{jl} = -w_{lj}$ and $t'_{jl} = -t'_{lj}$ are defined according to the orientation of nearest- and next-nearest-neighbor bonds, as illustrated in Fig. 4: $t_{jl} = t$, $w_{jl} = w$, and $t'_{jl} = t'$ if the corresponding arrow points from l to j and the opposite sign if the arrow points from j to l. The Hamiltonian in Eq. (14) is invariant under time reversal, $TiT^{-1} = -i$, $T\Psi_j T^{-1} = -i\sigma^y \Psi_j$, but breaks reflection and spin-rotational symmetries. Hamiltonians similar to Eq. (14) appear in the context of noncentrosymmetric superconductors [62,63]. Note that t and w alone break the sublattice inversion symmetry P: $t_{jl} \mapsto t_{lj}$, $w_{jl} \mapsto w_{lj}$, but a nonzero next-nearest-neighbor coupling t' is required to break the inversionlike symmetry

$$\text{P}': \quad t_{jl} \mapsto t_{lj}, \quad w_{jl} \mapsto w_{lj}, \quad t'_{jl} \mapsto t'_{lj},$$

$$\text{P}' \; \Psi_j (\text{P}')^{-1} = \begin{cases} \Psi_j & \text{if } j \in \text{sublattice A}, \\ -\Psi_j & \text{if } j \in \text{sublattice B}. \end{cases} \tag{16}$$

It is convenient to use the electron operators $\psi_{j\uparrow}$ and $\psi_{j\downarrow}$ to define four Majorana fermions by [52]

$$\Psi_j = \frac{1}{2} \begin{pmatrix} \mathbb{1}_2 & i\mathbb{1}_2 \\ -i\sigma^y & -\sigma^y \end{pmatrix} \zeta_j, \tag{17}$$

where $\mathbb{1}_2$ is the 2×2 identity matrix and $\zeta_j = (\zeta_j^1, \zeta_j^2, \zeta_j^3, \zeta_j^4)^T$, with ζ_j^μ obeying $\{\zeta_j^\mu, \zeta_l^\nu\} = 2\delta_{jl}\delta^{\mu\nu}$. More explicitly, we have

$$\begin{aligned}
\zeta_j^1 &= \psi_{j\uparrow} + \psi_{j\uparrow}^\dagger, \\
\zeta_j^2 &= \psi_{j\downarrow} + \psi_{j\downarrow}^\dagger, \\
\zeta_j^3 &= -i(\psi_{j\uparrow} - \psi_{j\uparrow}^\dagger), \\
\zeta_j^4 &= -i(\psi_{j\downarrow} - \psi_{j\downarrow}^\dagger).
\end{aligned} \tag{18}$$

Time reversal acts on these Majorana fermions as

$$T: \zeta_j^1 \mapsto \zeta_j^2, \; \zeta_j^2 \mapsto -\zeta_j^1, \; \zeta_j^3 \mapsto \zeta_j^4, \; \zeta_j^4 \mapsto -\zeta_j^3. \tag{19}$$
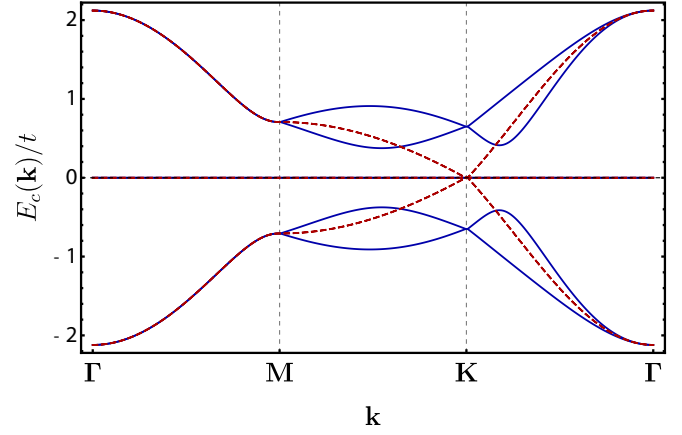

FIG. 5. Dispersion relation of itinerant electrons described by H_c in Eq. (14). Here we set $t = w$ and consider two values of the next-nearest-neighbor coupling: $t' = 0$ (dashed line) and $t' = t/2$ (solid line). The zero-energy flat bands are related to the ζ^1 and ζ^2 modes.

The Hamiltonian for the itinerant electrons can then be written as

$$\begin{aligned}
H_c = i \sum_{\langle jl \rangle} &\left[t_{jl}(\zeta_j^3 \zeta_l^4 + \zeta_j^4 \zeta_l^3) + w_{jl}(\zeta_j^3 \zeta_l^3 - \zeta_j^4 \zeta_l^4) \right] \\
&+ i \sum_{\langle\langle jl \rangle\rangle} t'_{jl}(\zeta_j^3 \zeta_l^4 + \zeta_j^4 \zeta_l^3).
\end{aligned} \tag{20}$$

In this form, it is clear that there are two Majorana fermions at each site, ζ_j^1 and ζ_j^2, which commute with H_c. We have defined the conduction electron Hamiltonian this way so that we can later hybridize these zero-energy Majorana modes with the Majorana fermions in the quadrupolar spin liquid when we turn on the Kondo coupling.

We can diagonalize H_c by taking the Fourier transform of the fermion operators. We obtain the dispersion relations

$$\begin{aligned}
E_c(\mathbf{k}) = \pm \big[(t^2 + w^2)|f(\mathbf{k})|^2 + \Delta_0^2(\mathbf{k}) \\
\pm 2w|\Delta_0(\mathbf{k})f(\mathbf{k})| \big]^{1/2},
\end{aligned} \tag{21}$$

where we define the functions $f(\mathbf{k}) = e^{i\mathbf{k}\cdot\mathbf{n}_1} + e^{i\mathbf{k}\cdot\mathbf{n}_2} + 1$ and $\Delta_0(\mathbf{k}) = -2t' \sum_{\gamma=1}^3 \sin(\mathbf{k}\cdot\boldsymbol{\delta}_\gamma)$, with $\boldsymbol{\delta}_1 = \mathbf{n}_2$, $\boldsymbol{\delta}_2 = -\mathbf{n}_1$, and $\boldsymbol{\delta}_3 = \mathbf{n}_1 - \mathbf{n}_2$. In the Majorana fermion basis, these bands are associated with ζ^3 and ζ^4, whereas the ζ^1 and ζ^2 fermions appear in the spectrum as zero-energy flat bands, see Fig. 5. The gap in the $\zeta^{3,4}$ sector is of order $|t'|$ if $|t'| \ll |t|, |w|$. We are mainly interested in the regime $|t'| \sim |t| \sim |w| \gg |K|, |\lambda|$, in which this gap is much larger than the interaction energy scale for the spin liquid. In this limit, we can project out the $\zeta^{3,4}$ sector and the low-energy physics is governed by the coupling between the $\zeta^{1,2}$ modes of the conduction electrons and the localized spins.

B. Octupolar Kondo coupling

We now look for an onsite interaction that couples electrons to local moments and preserves time reversal symmetry. First, we note that the projection of the electron spin operator

onto the sector of $\zeta^{1,2}$ Majorana fermions is given by

$$\mathcal{P}_{12}\Psi_j^\dagger \boldsymbol{\sigma}\Psi_j\mathcal{P}_{12} = \tfrac{1}{2}\Psi_j^\dagger(\sigma^y - \rho^y)\Psi_j\hat{\mathbf{y}}$$
$$= -i\zeta_j^1\zeta_j^2\hat{\mathbf{y}}, \qquad (22)$$

where $\mathcal{P}_{12}$ is the projection operator. Note that only the y component of the spin operator remains after the projection; this is possible because the spin-rotational symmetry is broken in the Hamiltonian in Eq. (14). If the superconducting gap in the $\zeta^{3,4}$ sector far exceeds all other energy scales, the operator in Eq. (22) is the only single-site electron operator active at low energies. We then consider the Kondo-like coupling

$$H_K = \frac{J_K}{2}\sum_j \Psi_j^\dagger(\sigma^y - \rho^y)\Psi_j T_j^{xyz}. \qquad (23)$$

This interaction involves the octupole moment $T_j^{xyz} \propto \tau_j^y$ of the localized spins. In terms of Majorana fermions, we have

$$H_K = J_K\sum_j \zeta_j^1\zeta_j^2\theta_j^x\theta_j^z. \qquad (24)$$

Note that the condition that the Kondo-like coupling must respect the conservation of the bond operators $\hat{u}_{\langle jl\rangle_\gamma}$ prevents us from coupling the projection of the electron spin operator in Eq. (22) to the dipole moments $\mathbf{J}_j$ of the localized spins, see Table I. We thus expect the coupling in Eq. (23) to arise from more microscopic models as the leading interaction between itinerant and localized electrons at energy scales far below the superconducting gap shown in Fig. 5 and the gap for changing the flux configuration in the spin liquid.

To solve the Hamiltonian in Eq. (13), we note that we can pair the θ_j^z Majorana fermion with either ζ_j^1 or ζ_j^2 to define the $\mathbb{Z}_2$ operators

$$\hat{v}_j = -i\zeta_j^{\mu_j}\theta_j^z, \qquad (25)$$

where $\mu_j \in \{1, 2\}$ can be chosen independently at each site. It is straightforward to verify that these operators commute not only with one another but also with the bond operators $\hat{u}_{\langle ij\rangle_\gamma}$ of the spin liquid and with the total Hamiltonian in Eq. (13). Thus, $\hat{v}_j$ are conserved quantities and we can replace them by the eigenvalues ± 1 to obtain a quadratic Hamiltonian in the remaining Majorana fermions. Remarkably, a finite expectation value of the $\hat{v}_j$ operators implies a hybridization between physical Majorana fermions defined from the conduction electrons and emergent Majorana fermions in the spin liquid. This type of hybridization has appeared in the literature as an order parameter for odd-frequency pairing in heavy-fermion superconductors [51,52].

Since time reversal exchanges ζ^1 and ζ^2, see Eq. (19), the choice of $\mu_j = 1, 2$ for each $\hat{v}_j$ breaks time reversal symmetry spontaneously. Thus, the Kondo coupling to the octupole moment of the spin liquid induces unconventional, time-reversal-symmetry-breaking superconductivity. To discuss the possible superconducting states, we must first assign values to the $\mathbb{Z}_2$ variables. We consider two states that respect the translational symmetry of the honeycomb lattice: the uniform or "ferro" (F) configuration

$$\hat{v}_j^{\mathrm{F}} = -i\zeta_j^1\theta_j^z = 1 \quad \forall j, \qquad (26)$$

and the staggered or "antiferro" (AF) configuration

$$\hat{v}_j^{\mathrm{AF}} = \begin{cases} -i\zeta_j^1\theta_j^z = 1, & \text{if } j \in \text{ sublattice A}, \\ -i\zeta_j^2\theta_j^z = 1, & \text{if } j \in \text{ sublattice B}. \end{cases} \qquad (27)$$

Changing the sign of $\hat{v}_j$ does not affect any physical observables, due to the gauge symmetry $(\eta_j^\alpha, \theta_j^\alpha) \mapsto (-\eta_j^\alpha, -\theta_j^\alpha)$ of the Majorana fermion representation in the spin liquid sector. The Kondo coupling for F and AF configurations becomes, respectively,

$$H_K^{\mathrm{F}} = iJ_K\sum_j \zeta_j^2\theta_j^x, \qquad (28)$$

$$H_K^{\mathrm{AF}} = iJ_K\sum_{j\in A} \zeta_j^2\theta_j^x - iJ_K\sum_{j\in B} \zeta_j^1\theta_j^x. \qquad (29)$$

In order to obtain the energy spectrum with finite Kondo interaction, we define the spinors

$$\Upsilon_{\mathrm{F}}(\mathbf{k}) = \begin{pmatrix} \theta_A^x(\mathbf{k}) \\ \theta_B^x(\mathbf{k}) \\ \theta_A^y(\mathbf{k}) \\ \theta_B^y(\mathbf{k}) \\ \zeta_A^2(\mathbf{k}) \\ \zeta_B^2(\mathbf{k}) \end{pmatrix}, \quad \Upsilon_{\mathrm{AF}}(\mathbf{k}) = \begin{pmatrix} \theta_A^x(\mathbf{k}) \\ \theta_B^x(\mathbf{k}) \\ \theta_A^y(\mathbf{k}) \\ \theta_B^y(\mathbf{k}) \\ \zeta_A^2(\mathbf{k}) \\ -\zeta_B^1(\mathbf{k}) \end{pmatrix}, \qquad (30)$$

which contain the Majorana fermions that acquire a dispersion at low energies. The total Hamiltonian has the form

$$\mathcal{P}_{12}H^{\mathrm{F/AF}}\mathcal{P}_{12} = \sum_{\mathbf{k}} \Upsilon_{\mathrm{F/AF}}^\dagger(\mathbf{k})\mathcal{H}(\mathbf{k})\Upsilon_{\mathrm{F/AF}}(\mathbf{k}), \qquad (31)$$

where the antisymmetric matrix $\mathcal{H}(\mathbf{k})$ is the same for both uniform and staggered configurations:

$$\mathcal{H}(\mathbf{k}) = \begin{pmatrix} \mathcal{H}_s(\mathbf{k}) & V^\dagger \\ V & \mathbb{0}_2 \end{pmatrix}, \qquad (32)$$

with $\mathbb{0}_2$ the 2×2 null matrix,

$$\mathcal{H}_s(\mathbf{k}) = \begin{pmatrix} 0 & 0 & i\lambda & 0 \\ 0 & 0 & 0 & i\lambda \\ -i\lambda & 0 & 0 & ig(\mathbf{k}) \\ 0 & -i\lambda & -ig^*(\mathbf{k}) & 0 \end{pmatrix}, \qquad (33)$$

and

$$V = \begin{pmatrix} -iJ_K & 0 & 0 & 0 \\ 0 & -iJ_K & 0 & 0 \end{pmatrix}. \qquad (34)$$

Thus, F and AF states share the same energy spectrum illustrated in Fig. 6. We see that the Majorana fermions that appear in the Kondo coupling Eqs. (28) and (29) give rise to a gapless band structure with a Dirac node at the K point. This represents the dispersion of the Bogoliubov quasiparticles in this nodal superconductor. There are no zero-energy flat bands left. The dispersion relations for the decoupled $\zeta^{3,4}$ modes are given by Eq. (21) and appear at much higher energies provided that $|t| \sim |t'| \sim |w| \gg |K|, |\lambda|, |J_K|$.

Since we obtain the same spectrum for F and AF configurations, these two states have exactly the same ground state energy. This degeneracy can be traced back to a local SO(2) symmetry of the exactly solvable model. We can regard ζ_j^1 and ζ_j^2 as the real and imaginary parts of a complex fermion
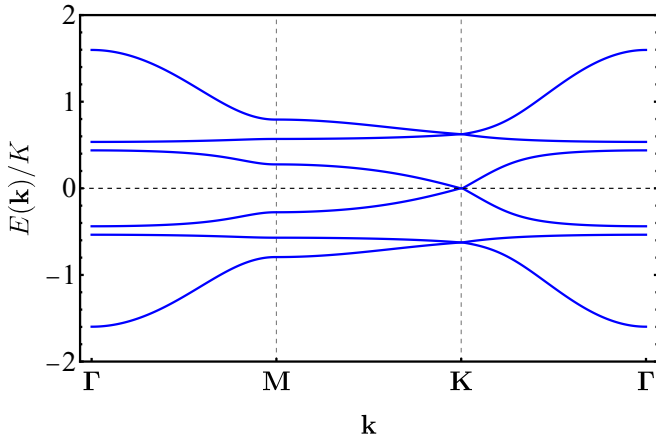
FIG. 6. Dispersion relation of Majorana fermions in both F and AF configurations of the coupled system. Here we set $\lambda/K = 0.75$ and $J_K/K = 1$. The bands associated with the decoupled ζ^3 and ζ^4 Majorana fermions appear at much higher energies and are not shown.

defined at each site. The choice of real and imaginary parts can be parametrized by a rotation in the complex plane, i.e., the phase of the complex fermion. This choice is arbitrary and can be made locally at each site because these Majorana modes only appear in the Kondo coupling Eq. (24). As we shall discuss in Sec. V, the degeneracy between F and AF states is lifted once we add integrability-breaking perturbations that couple ζ^1 and ζ^2 at different sites and remove the local SO(2) symmetry.

Interestingly, despite the spontaneous time reversal symmetry breaking, the local magnetization vanishes exactly in the ground state of the exactly solvable model:

$$\langle \Psi_j^\dagger \boldsymbol{\sigma} \Psi_j \rangle = 0, \quad \langle \mathbf{J}_j \rangle = 0. \tag{35}$$

The reason is that both the electron and local moment spin operators contain Majorana fermions absorbed into the $\mathbb{Z}_2$ operators, whose action on a given eigenstate changes the sector of $\mathbb{Z}_2$ fluxes. Local time-reversal-odd operators that acquire a nonzero expectation value must involve a product of electron and local-moment operators, for instance,

$$\langle O_j^{x^2-y^2} \Psi_j^\dagger \sigma^y \Psi_j \rangle \sim \langle \theta_j^y \theta_j^z \zeta_j^1 \zeta_j^2 \rangle$$
$$\sim \langle \zeta_j^1 \theta_j^z \rangle \langle \zeta_j^2 \theta_j^y \rangle \neq 0, \tag{36}$$

where the factor $\langle \zeta_j^2 \theta_j^y \rangle$ is nonzero because $\lambda \neq 0$ mixes θ_j^y with θ_j^x and the operator $\zeta_j^2 \theta_j^x$ appears in the Kondo coupling in Eq. (28). This provides an example of a composite order parameter [54,64–71] or vestigial order [72].

IV. EFFECTIVE ACTION FOR ELECTRONS IN THE COUPLED SYSTEM

In this section, we investigate the effect of the octupolar Kondo coupling on the superconducting properties of the coupled system. Since the Hamiltonian becomes quadratic after fixing the values of the $\mathbb{Z}_2$ variables, we can integrate out the Majorana fermions of the quadrupolar spin liquid to derive an exact effective action for the conduction electrons. We are mainly interested in the pairing amplitudes generated by the Kondo coupling which manifest the breaking of time reversal symmetry. We find that, while the uniform and staggered configurations are degenerate within the exactly solvable model, they produce different superconducting order parameters because the physical Majorana fermions ζ^1 and ζ^2 are associated with different electronic spin states, see Eq. (18). More details of the calculations are given in Appendix C.

A. Superconducting state in the F configuration

For the uniform state with the Kondo interaction H_K^F in Eq. (28), the effective action obtained after integrating out the Majorana fermions θ^x and θ^y has the form

$$\mathcal{S}_F = \sum_{\mathbf{k},\omega_n} \Psi^\dagger(\mathbf{k}, i\omega_n)[i\omega_n - \mathcal{H}_c(\mathbf{k}) - \Sigma_F(\mathbf{k}, i\omega_n)]\Psi(\mathbf{k}, i\omega_n), \tag{37}$$

where ω_n are Matsubara frequencies and $\Psi(\mathbf{k}, i\omega_n)$ is the Balian-Werthamer spinor in momentum-frequency space:

$$\Psi(\mathbf{k}, i\omega_n) = \begin{pmatrix} \Psi_A(\mathbf{k}, i\omega_n) \\ \Psi_B(\mathbf{k}, i\omega_n) \end{pmatrix}, \tag{38}$$

with

$$\Psi_{A/B}(\mathbf{k}, i\omega_n) = \begin{pmatrix} \psi_{A/B}(\mathbf{k}, i\omega_n) \\ -i\sigma^y[\psi_{A/B}^\dagger(-\mathbf{k}, -i\omega_n)]^T \end{pmatrix}. \tag{39}$$

Here $\mathcal{H}_c(\mathbf{k})$ is the matrix obtained by Fourier transforming H_c in Eq. (14), see Appendix C. The self-energy $\Sigma_F(\mathbf{k}, i\omega_n)$ is due to the hybridization of the conduction electrons with the Majorana fermions of the spin liquid and is of order J_K^2.

The effective action in Eq. (37) contains three terms: a normal (N), a superconducting (SC), and a resonant-exchange (RE) part. The N and RE parts are written explicitly in Appendix C. Here we discuss only the contribution from the Kondo coupling to the SC part, which has the form

$$\delta \mathcal{S}_F^{SC} = \sum_{\mathbf{k},\omega_n} \sum_{b,b'} \left[\psi_b^T(-\mathbf{k}, -i\omega_n)\sigma^y \Delta_{bb'}^{SC}(\mathbf{k}, i\omega_n)\psi_{b'}(\mathbf{k}, i\omega_n) + \text{H.c.} \right], \tag{40}$$

where b, b' are sublattice indices. The induced pairing functions are given by

$$\Delta_{AA}^{SC}(\mathbf{k}, i\omega_n) = \frac{J_K^2}{2} \frac{\omega_n(\omega_n^2 + |g(\mathbf{k})|^2 + \lambda^2)\sigma^+}{(\omega_n^2 + \lambda^2)^2 + |g(\mathbf{k})|^2\omega_n^2},$$

$$\Delta_{AB}^{SC}(\mathbf{k}, i\omega_n) = -\frac{J_K^2}{2} \frac{\lambda^2 g(\mathbf{k})\sigma^+}{(\omega_n^2 + \lambda^2)^2 + |g(\mathbf{k})|^2\omega_n^2},$$

$$\Delta_{BA}^{SC}(\mathbf{k}, i\omega_n) = \frac{J_K^2}{2} \frac{\lambda^2 g^*(\mathbf{k})\sigma^+}{(\omega_n^2 + \lambda^2)^2 + |g(\mathbf{k})|^2\omega_n^2},$$

$$\Delta_{BB}^{SC}(\mathbf{k}, i\omega_n) = \frac{J_K^2}{2} \frac{\omega_n(\omega_n^2 + |g(\mathbf{k})|^2 + \lambda^2)\sigma^+}{(\omega_n^2 + \lambda^2)^2 + |g(\mathbf{k})|^2\omega_n^2}, \tag{41}$$

where $\sigma^\pm = (\sigma^x \pm i\sigma^y)/2$. Therefore, the Kondo coupling gives rise to triplet pairing with both even- and odd-frequency amplitudes. Exactly at the K point, where $g(\mathbf{k})$ vanishes for $K_\gamma = K$, the AB and BA components vanish, whereas the AA and BB components scale linearly with frequency,

$\Delta_{bb}^{SC} \sim (J_K/\lambda)^2 \omega_n \sigma^+$ for $|\omega_n| \ll |\lambda|$. This result bears a close resemblance to mean-field theories for related Kondo lattice models [52,54,73].

B. Superconducting state in the AF configuration

We repeat the procedure of Sec. IV A for the staggered state with the Kondo interaction given in Eq. (29). The effective action in this case also exhibits N, SC, and RE contributions. The superconducting part generated by the Kondo coupling in the AF case reads

$$\delta\mathcal{S}_{AF}^{SC} = \sum_{\mathbf{k},\omega_n} \sum_{b,b'} \left[\psi_b^T(-\mathbf{k}, -i\omega_n) \sigma^y \tilde{\Delta}_{bb'}^{SC}(\mathbf{k}, i\omega_n) \psi_{b'}(\mathbf{k}, i\omega_n) \right.$$
$$\left. + \text{H.c.} \right], \tag{42}$$

where

$$\tilde{\Delta}_{AA}^{SC}(\mathbf{k}, i\omega_n) = \frac{J_K^2}{2} \frac{\omega_n(\omega_n^2 + |g(\mathbf{k})|^2 + \lambda^2)\sigma^+}{(\omega_n^2 + \lambda^2)^2 + |g(\mathbf{k})|^2\omega_n^2},$$

$$\tilde{\Delta}_{AB}^{SC}(\mathbf{k}, i\omega_n) = \frac{J_K^2}{4} \frac{\lambda^2 g(\mathbf{k})(\mathbb{1}_2 + \sigma^z)}{(\omega_n^2 + \lambda^2)^2 + |g(\mathbf{k})|^2\omega_n^2},$$

$$\tilde{\Delta}_{BA}^{SC}(\mathbf{k}, i\omega_n) = \frac{J_K^2}{4} \frac{\lambda^2 g^*(\mathbf{k})(\mathbb{1}_2 - \sigma^z)}{(\omega_n^2 + \lambda^2)^2 + |g(\mathbf{k})|^2\omega_n^2},$$

$$\tilde{\Delta}_{BB}^{SC}(\mathbf{k}, i\omega_n) = -\frac{J_K^2}{2} \frac{\omega_n(\omega_n^2 + |g(\mathbf{k})|^2 + \lambda^2)\sigma^-}{(\omega_n^2 + \lambda^2)^2 + |g(\mathbf{k})|^2\omega_n^2}. \tag{43}$$

These pairing functions also involve a mixture of even- and odd-frequency pairing. However, they are markedly different from those in the uniform configuration, since now the AB and BA components exhibit a superposition of singlet and triplet pairings. Moreover, the AA and BB components differ in the spin dependence of the triplet pairing. At the K point, $\Delta_{AA}^{SC} \sim (J_K/\lambda)^2 \omega_n \sigma^+$ for the A sublattice, but $\Delta_{BB}^{SC} \sim (J_K/\lambda)^2 \omega_n \sigma^-$ for the B sublattice.

V. INTEGRABILITY-BREAKING PERTURBATIONS

In this section, we go beyond the exactly solvable model to examine whether perturbations may lift the degeneracy between the F and AF configurations. Rather than discuss all symmetry-allowed perturbations, we focus on the effects of additional quadratic terms in the conduction electron Hamiltonian that involve the Majorana fermions ζ^1 and ζ^2. We consider

$$\delta H_c = i \sum_{\langle jl \rangle} \left[\delta t_{jl} \left(\zeta_j^1 \zeta_l^2 + \zeta_j^2 \zeta_l^1 \right) + \delta w_{jl} \left(\zeta_j^1 \zeta_l^1 - \zeta_j^2 \zeta_l^2 \right) \right]$$
$$+ i \sum_{\langle\langle jl \rangle\rangle} \left[\delta t'_{jl} \left(\zeta_j^1 \zeta_l^2 + \zeta_j^2 \zeta_l^1 \right) + \delta w'_{jl} \left(\zeta_j^1 \zeta_l^1 - \zeta_j^2 \zeta_l^2 \right) \right], \tag{44}$$

where we fix the values of $\delta t_{jl} = \pm \delta t$, $\delta w_{jl} = \pm \delta w$, $\delta t'_{jl} = \pm \delta t'$ and $\delta w'_{jl} = \pm \delta w'$ according to the orientation of the nearest and next-nearest-neighbor links as explained in Sec. III A. In terms of the Balian-Werthamer spinor [see

Eq. (15)], δH_c assumes the form

$$\delta H_c = \sum_{\langle jl \rangle} \Psi_j^\dagger M_{jl} \Psi_l + \sum_{\langle\langle jl \rangle\rangle} \Psi_j^\dagger M'_{jl} \Psi_l, \tag{45}$$

with

$$M_{jl} = i\delta t_{jl}(\sigma^x \rho^z - \sigma^z \rho^x) + i\delta w_{jl}(\sigma^z \rho^z + \sigma^x \rho^x),$$
$$M'_{jl} = i\delta t'_{jl}(\sigma^x \rho^z - \sigma^z \rho^x) + i\delta w'_{jl}(\sigma^z \rho^z + \sigma^x \rho^x). \tag{46}$$

Since the $\mathbb{Z}_2$ operators $\hat{v}_j$ defined in Eq. (25) do not commute with δH_c, this perturbation breaks the integrability of the model. Here we shall assume that $|\delta t|, |\delta w|, |\delta t'|, |\delta w'| \ll |K|, |\lambda|, |J_K|$ so that the $\mathbb{Z}_2$ variables are still good order parameters with expectation value $\langle \hat{v}_j \rangle \approx 1$. One consequence of the perturbation is that the Majorana fermions absorbed into $\hat{v}_j$ must acquire a small dispersion. Nevertheless, as long as the latter remain gapped, this should not affect qualitative properties of the low-energy spectrum discussed in the following.

In the spirit of first-order perturbation theory, we project δH_c onto the low-energy subspace where the Majorana fermions contained in $\hat{v}_j$ are gapped out and cannot be excited. For the F configuration, this rules out the terms involving ζ^1 altogether. As a result, we obtain the projected perturbation

$$\delta H_c^F = -i \sum_{\langle jl \rangle} \delta w_{jl} \zeta_j^2 \zeta_l^2 - i \sum_{\langle\langle jl \rangle\rangle} \delta w'_{jl} \zeta_j^2 \zeta_l^2. \tag{47}$$

In contrast, in the AF configuration the fermionic excitations related to ζ^1 become gapped only in sublattice A, while those related to ζ^2 are gapped in sublattice B. Consequently, the projection of δH_c for the AF state yields

$$\delta H_c^{AF} = i \sum_{\substack{\langle jl \rangle \\ j \in B}} \delta t_{jl} \zeta_j^1 \zeta_l^2 + i \sum_{\substack{\langle\langle jl \rangle\rangle \\ j \in B}} \delta w'_{jl} \zeta_j^1 \zeta_l^1 - i \sum_{\substack{\langle\langle jl \rangle\rangle \\ j \in A}} \delta w'_{jl} \zeta_j^2 \zeta_l^2. \tag{48}$$

Note that both δH_c^F and δH_c^{AF} remove the local SO(2) symmetry that exchanges ζ_j^1 and ζ_j^2, see Sec. III B.

We add the terms in Eqs. (47) and (48) to the Hamiltonian for the coupled system in the F and AF configurations, respectively, and recalculate the spectrum by taking the Fourier transform of the Majorana fermion operators. The dispersion relations are shown in Fig. 7. We find that the degeneracy between F and AF states is lifted by a finite next-nearest-neighbor coupling $\delta w'$. The latter produces a gap in the excitation spectrum for the F state, while for the AF state it turns the Dirac point into a Bogoliubov Fermi surface [56]. The ground state energies of the two configurations are now clearly different, and either state can have lower energy depending on the values of δt, δw, and $\delta w'$.

We also investigated the presence of edge states for the perturbed superconducting states on a strip geometry. The results are presented in Fig. 8. For both F and AF states, there exist pairs of gapless edge modes due to the nontrivial topological nature of the phase. The perturbed F state is a gapped superconductor with counterpropagating chiral edge modes localized at opposite edges of the strip. On the other hand, the AF state has edge states that propagate in the same direction and whose equilibrium current is compensated by
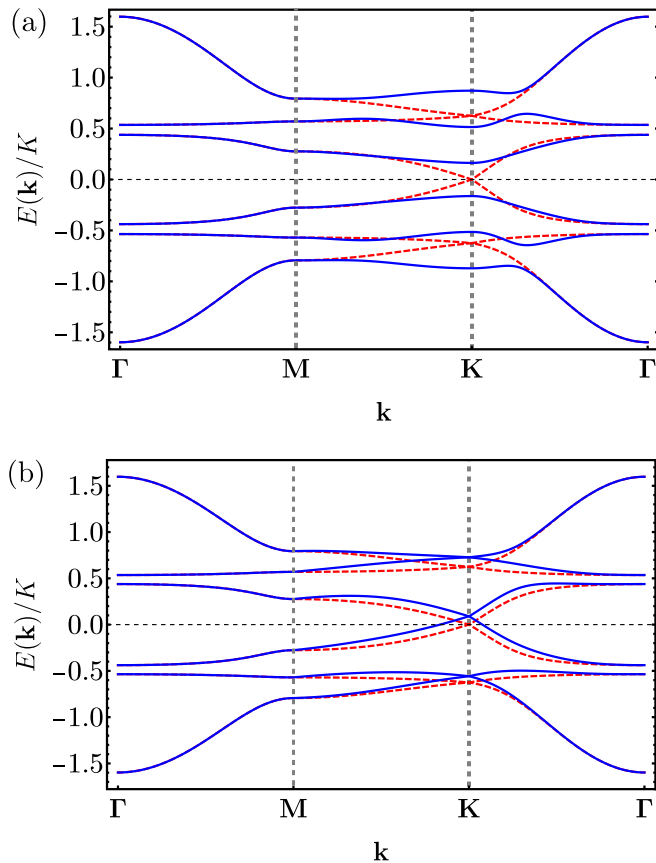
FIG. 7. Low-energy bands of the coupled system including the integrability-breaking perturbations in the (a) F configuration and (b) AF configuration. Here we use $\lambda/K = 0.75$, $J_K/K = 1$, and $\delta t = \delta w = 0$. The solid lines show the result for $\delta w'/K = 0.2$, which can be compared with the dispersion for the exactly solvable model ($\delta w' = 0$) given by the dashed lines. For the F state, a small $\delta w'$ opens a gap at the K point. For the AF state, it induces the formation of a Bogoliubov Fermi surface.
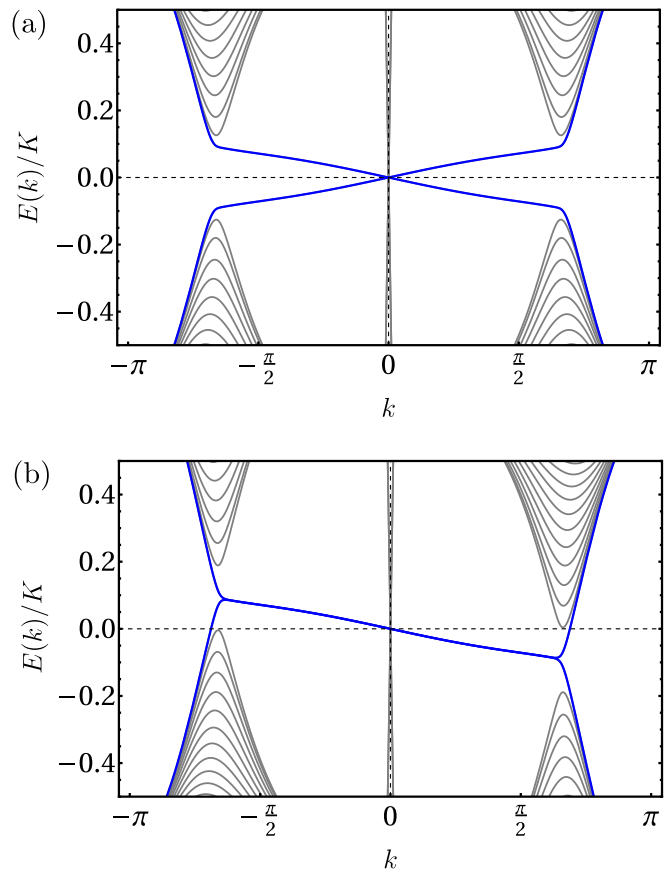

FIG. 8. Band structure of the perturbed model for the coupled system with open boundary conditions in the *y* direction and width $W = 60$ unit cells. Here we set $J_K/K = 1$, $\lambda/K = 0.75$, and $\delta t/K = \delta w/K = \delta w'/K = 0.1$. Panel (a) shows the spectrum for the F state. The blue lines highlight the gapless edge states associated with the low-energy Majorana fermions. We also show the pair of edge states associated with the $\zeta^{3,4}$ sector of the conduction electrons, whose bulk excitations appear at much higher energies. The parameters in this sector are set to $t/K = w/K = 10$ and $t'/K = 5$. Panel (b) shows the spectrum for the AF state. In this case we find antichiral edge states.

that of the gapless bulk modes. This is a superconducting version of the antichiral edge states discussed in Ref. [57]. Note that both types of band structures shown in Fig. 8 are only possible once time reversal symmetry is broken.

VI. CONCLUSIONS

We proposed an exactly solvable model for interacting $j_{\text{eff}} = \frac{3}{2}$ local moments on the honeycomb lattice. Our proposal is guided by symmetry properties and by a Majorana fermion representation of the multipole operators. We first analyzed a time-reversal-invariant spin model that includes bond-dependent quadrupole-quadrupole interactions and a single-ion anisotropy term. To obtain a solvable spin Hamiltonian with no zero-energy flat bands, we added terms that break time reversal symmetry explicitly and found a gapped chiral spin liquid.

We also investigated the coupling of the time-reversal-invariant quadrupolar spin liquid to a superconductor, with the goal of constructing an exactly solvable model in which the Majorana fermions in the spin liquid hybridize with itinerant electrons. The conserved $\mathbb{Z}_2$ variables defined in the octupolar

Kondo coupling are related to the order parameter for odd-frequency pairing in heavy-fermion superconductors [51,52]. Indeed, we find that this Kondo coupling breaks time reversal symmetry spontaneously and generates odd-frequency pairing in the effective action for the conduction electrons. The result within the exactly solvable model is a gapless time-reversal-symmetry-breaking superconductor. Perturbing the model with integrability breaking terms, we obtained either a gapped chiral superconductor or a Bogoliubov Fermi surface state, both of which exhibit topologically protected (chiral or antichiral) edge states.

Our results illustrate the possibility of inducing new topological phases by coupling two subsystems which may or may not have topological properties by themselves. This observation is in line with the bulk topological proximity effect introduced in Refs. [74,75] and with the proposal of topological superconductivity in the Kondo-Kitaev model [44]. Also noteworthy is the recent experimental evidence

for odd-frequency superconductivity at the interface between a topological insulator and a conventional superconductor [76]. While in this work we have focused on analyzing the properties of an exactly solvable toy model, an interesting open question is whether one could tune more realistic effective Hamiltonians for spin-orbit-coupled materials to the vicinity of this integrable point. Besides $j_{\text{eff}} = \frac{3}{2}$ systems, the spin-orbital physics discussed here could be relevant to correlated Moiré systems [77,78] and heterostructures [79] with orbital/valley degrees of freedom.

APPENDIX A: MAJORANA FERMION REPRESENTATION

In this Appendix, we discuss the transformation of the Majorana fermions in the spin liquid under time reversal. At each site, we can combine the six Majorana fermions $(\eta^\alpha, \theta^\alpha)$ to define three complex fermions:

$$c^x = \tfrac{1}{2}(\eta^x - i\theta^x),$$
$$c^y = \tfrac{1}{2}(\eta^y - i\theta^y),$$
$$c^z = \tfrac{1}{2}(\eta^z - i\theta^z), \tag{A1}$$

which obey $\{c^\alpha, (c^\beta)^\dagger\} = \delta^{\alpha\beta}$. States in this Fock space are specified by $|n_x, n_y, n_z\rangle$, where $n_\alpha \in \{0, 1\}$ are the fermion occupation numbers. Thus, this representation generates eight states, which is twice the size of the physical Hilbert space for spin 3/2. We can represent the four eigenstates of J^z by identifying

$$\left|\tfrac{3}{2}\right\rangle = |0, 0, 0\rangle \equiv |\varnothing\rangle,$$
$$\left|\tfrac{1}{2}\right\rangle = |1, 1, 0\rangle = (c^x)^\dagger (c^y)^\dagger |\varnothing\rangle,$$
$$\left|-\tfrac{1}{2}\right\rangle = |0, 1, 1\rangle = (c^y)^\dagger (c^z)^\dagger |\varnothing\rangle,$$
$$\left|-\tfrac{3}{2}\right\rangle = |1, 0, 1\rangle = (c^x)^\dagger (c^z)^\dagger |\varnothing\rangle. \tag{A2}$$

This corresponds to imposing the parity constraint

$$(2n_x - 1)(2n_y - 1)(2n_z - 1) = -1, \tag{A3}$$

which in terms of Majorana fermions becomes Eq. (6).

Since time reversal acts on the spin-3/2 states as

$$T\left|\tfrac{3}{2}\right\rangle = \left|-\tfrac{3}{2}\right\rangle, \quad T\left|\tfrac{1}{2}\right\rangle = -\left|-\tfrac{1}{2}\right\rangle,$$
$$T\left|-\tfrac{1}{2}\right\rangle = \left|\tfrac{1}{2}\right\rangle, \quad T\left|-\tfrac{3}{2}\right\rangle = -\left|\tfrac{3}{2}\right\rangle, \tag{A4}$$

we postulate that time reversal is equivalent to a particle-hole transformation for fermions c^x and c^z, such that $Tc^{x,z}T^{-1} =$

$(c^{x,z})^\dagger$ and $T|0, 0, 0\rangle = |1, 0, 1\rangle$. We can then check that

$$T\left|-\tfrac{3}{2}\right\rangle = T(c^x)^\dagger(c^z)^\dagger|\varnothing\rangle$$
$$= c^x c^z T|\varnothing\rangle$$
$$= c^x c^z (c^x)^\dagger(c^z)^\dagger|\varnothing\rangle$$
$$= -|\varnothing\rangle, \tag{A5}$$

as expected. Likewise, it is straightforward to verify the time reversal transformation of the $|\pm\tfrac{1}{2}\rangle$ states. The rule of particle-hole transformation for c^x and c^z but not for c^y is equivalent to applying complex conjugation and taking $\theta^y \mapsto -\theta^y$, as mentioned in Sec. II B.

APPENDIX B: GROUND STATE DEGENERACY OF THE TIME-REVERSAL-SYMMETRIC QUADRUPOLAR SPIN LIQUID

In this Appendix, we discuss the ground state degeneracy of the Hamiltonian in Eq. (4). First, consider the case $\lambda = 0$, in which the Hamiltonian commutes with the operators τ_j^y on every site. Using the representation of pseudospin and pseudo-orbital operators, we can write the Hamiltonian in the form

$$H_s(\lambda = 0) = 16K \sum_{\gamma=x,y,z} \sum_{\langle jl\rangle_\gamma} \tau_j^y \tau_l^y s_j^\gamma s_l^\gamma. \tag{B1}$$

We can replace the conserved quantities by their eigenvalues, $\tau_j^y = \tfrac{1}{2}\xi_j$, where $\xi_j \in \{\pm 1\}$, and obtain

$$H_s(\lambda = 0) = 4 \sum_{\gamma=x,y,z} \sum_{\langle jl\rangle_\gamma} K_{jl} s_j^\gamma s_l^\gamma, \tag{B2}$$

where $K_{jl} = K\xi_j\xi_l$. The Hilbert space can then be divided into sectors of $\{\xi_j\}$. Note that the product $\xi_j\xi_l$ determines the sign of the exchange coupling K_{jl} between the pseudospins on the bond $\langle jl\rangle_\gamma$. For instance, if we fix $\xi_j = 1 \,\forall j$, the model reduces to the homogeneous spin-1/2 Kitaev model. Moreover, the Kitaev model with opposite sign for the coupling is obtained in the sector with $\xi_j = 1$ for all sites j in sublattice A and $\xi_l = -1$ for all sites l in sublattice B. Importantly, ξ_j and ξ_l are eigenvalues of local physical operators, as opposed to gauge variables that arise in parton constructions.

We now show that every eigenstate in a given sector is degenerate with a state in another sector where the set $\{\xi_j\}$ differs only by a local change of the eigenvalues in a single bond. This implies an extensive degeneracy that scales with the number of bonds, which is manifested in the Majorana fermion representation through the presence of zero-energy flat bands in the spectrum of Fig. 2.

Consider that we start in a given sector, where Hamiltonian (B2) has a set of eigenstates $\{|\Psi_n(\{\xi_j\})\rangle\}$, and change to a different sector by inverting the sign of ξ_j and ξ_l on a single z bond. This transformation does not affect the sign of K_{jl} on that bond, but it flips the sign of the couplings of sites j and l to their nearest neighbors on x and y bonds. However, this sign change can be removed by applying a local π rotation around the z axis, which takes $s_j^{x,y} \mapsto -s_j^{x,y}$ and $s_l^{x,y} \mapsto -s_l^{x,y}$. This means that the Hamiltonian in the new sector is related to the original one by a canonical transformation, and to any eigenstate in the original sector there corresponds an eigenstate in the new sector with the same energy.

For $\lambda \neq 0$, the τ_j^y operators are no longer conserved, but one can verify that the local two-site operators $\tau_j^z \tau_l^z s_j^z s_l^z$, with j, l nearest neighbors on z bonds, commute with the Hamiltonian. In the Majorana fermion representation, these operators are written as $\frac{i}{4} u_{\langle jl \rangle_z} \theta_j^z \theta_l^z$. Thus, their conservation law is associated with the fact that the θ_j^z Majorana fermion does not appear in the Hamiltonian in Eq. (8). Let us denote the eigenvalues of $\tau_j^z \tau_l^z s_j^z s_l^z$ by $\frac{1}{16} \xi_{jl}$, where $\xi_{jl} \in \{\pm 1\}$. In a sector with fixed $\{\xi_{jl}\}$, we can write

$$s_j^z s_l^z = \xi_{jl} \tau_j^z \tau_l^z. \tag{B3}$$

The Hamiltonian in Eq. (4) can then be expressed in the form

$$H_s = 16K \sum_{\gamma = x,y} \sum_{\langle jl \rangle_\gamma} \tau_j^y \tau_l^y s_j^\gamma s_l^\gamma + 16K \sum_{\langle jl \rangle_z} \xi_{jl} \tau_j^y \tau_l^y \tau_j^z \tau_l^z - 2\lambda \sum_j \tau_j^z$$

$$= 16K \sum_{\gamma = x,y} \sum_{\langle jl \rangle_\gamma} \tau_j^y \tau_l^y s_j^\gamma s_l^\gamma - 4K \sum_{\langle jl \rangle_z} \xi_{jl} \tau_j^x \tau_l^x - 2\lambda \sum_j \tau_j^z. \tag{B4}$$

The argument for the degeneracy now is similar to the one given above. Suppose we flip the sign of a single ξ_{jl}. We can map the Hamiltonian in the new sector to the original one by applying a unitary transformation that takes $\tau_j^{x,y} \mapsto -\tau_j^{x,y}$ and $s_j^{x,y} \mapsto -s_j^{x,y}$ on site j only. Note that the π rotation acting on both pseudospins is necessary to preserve the sign of the first term in Eq. (B4). We conclude that also for $\lambda \neq 0$ there is an extensive degeneracy in the spectrum of H_s.

APPENDIX C: EFFECTIVE ACTION

In this Appendix, we provide details about the calculation of the effective action discussed in Sec. IV. The term $\mathcal{H}_c(\mathbf{k})$ in Eq. (37) is the Hamiltonian matrix obtained by Fourier transforming H_c in Eq. (14), which written as matrix in sublattice space becomes

$$\mathcal{H}_c(\mathbf{k}) = \frac{1}{2} \begin{pmatrix} \Delta_0(\mathbf{k})(\sigma^x \rho^z + \sigma^z \rho^x) & if(\mathbf{k})[t(\sigma^x \rho^z + \sigma^z \rho^x) + w(\sigma^z \rho^z - \sigma^x \rho^x)] \\ -if^*(\mathbf{k})[t(\sigma^x \rho^z + \sigma^z \rho^x) + w(\sigma^z \rho^z - \sigma^x \rho^x)] & -\Delta_0(\mathbf{k})(\sigma^x \rho^z + \sigma^z \rho^x) \end{pmatrix}. \tag{C1}$$

In this form, it is easy to see that $\mathcal{H}_c(\mathbf{k})$ already contains triplet pairing correlations. However, we want to address the contributions contained in the electron self-energy, which has the form

$$\Sigma_{\text{F/AF}}(\mathbf{k}, i\omega_n) = \mathcal{V}_{\text{F/AF}} \frac{1}{i\omega_n - \mathcal{H}_s(\mathbf{k})} \mathcal{V}_{\text{F/AF}}^\dagger, \tag{C2}$$

where $\mathcal{H}_s(\mathbf{k})$ is given in Eq. (33) and $\mathcal{V}_{\text{F/AF}}$ are hybridization matrices between the Balian-Werthamer spinor and the Majorana fermions in the spin liquid.

1. Uniform configuration

For the F state, the hybridization matrix is

$$\mathcal{V}_{\text{F}}^\dagger = \frac{iJ_K}{\sqrt{2}} \begin{pmatrix} 0 & 0 & 0 & 0 & 0 & 0 & 0 & 0 \\ 0 & 0 & 0 & 0 & 0 & 0 & 0 & 0 \\ 0 & -1 & 1 & 0 & 0 & 0 & 0 & 0 \\ 0 & 0 & 0 & 0 & 0 & -1 & 1 & 0 \end{pmatrix}. \tag{C3}$$

Substituting the above expression into Eq. (C2), we obtain the self-energy

$$\Sigma_{\text{F}}(\mathbf{k}, i\omega_n) = \frac{J_K^2}{2} (\mathbb{1}_4 - \boldsymbol{\sigma} \cdot \boldsymbol{\rho}) \otimes \mathcal{M}(\mathbf{k}, i\omega_n), \tag{C4}$$

where we introduce the matrix in sublattice space

$$\mathcal{M}(\mathbf{k}, i\omega_n) = \begin{pmatrix} i\Omega(\mathbf{k}, i\omega_n) & i\Gamma(\mathbf{k}, i\omega_n) \\ -i\Gamma^*(\mathbf{k}, i\omega_n) & i\Omega(\mathbf{k}, i\omega_n) \end{pmatrix}, \tag{C5}$$

with the following functions:

$$\Omega(\mathbf{k}, i\omega_n) = -\frac{\omega_n[\omega_n^2 + |g(\mathbf{k})|^2 + \lambda^2]}{2[(\omega_n^2 + \lambda^2)^2 + |g(\mathbf{k})|^2 \omega_n^2]}, \tag{C6}$$

$$\Gamma(\mathbf{k}, i\omega_n) = \frac{\lambda^2 g(\mathbf{k})}{2[(\omega_n^2 + \lambda^2)^2 + |g(\mathbf{k})|^2 \omega_n^2]}. \tag{C7}$$

As done in Ref. [52], we decompose $\Sigma_F(\mathbf{k}, i\omega_n)$ into three terms:

$$\Sigma_F(\mathbf{k}, i\omega_n) = \Sigma_F^N(\mathbf{k}, i\omega_n) + \Sigma_F^{SC}(\mathbf{k}, i\omega_n) + \Sigma_F^{RE}(\mathbf{k}, i\omega_n), \tag{C8}$$

where

$$\Sigma_F^N(\mathbf{k}, i\omega_n) = \frac{J_K^2}{2} \mathbb{1}_4 \otimes \mathcal{M}(\mathbf{k}, i\omega_n),$$

$$\Sigma_F^{SC}(\mathbf{k}, i\omega_n) = -\frac{J_K^2}{4}(\sigma^+\rho^- + \sigma^-\rho^+) \otimes \mathcal{M}(\mathbf{k}, i\omega_n),$$

$$\Sigma_F^{RE}(\mathbf{k}, i\omega_n) = -\frac{J_K^2}{2}\sigma^z\rho^z \otimes \mathcal{M}(\mathbf{k}, i\omega_n). \tag{C9}$$

Expressing the action in terms of the two-component spinors $\psi_{A/B}(\mathbf{k}, i\omega_n)$, we find the superconducting action and pairing function written in Eqs. (40) and (41), respectively.

Proceeding rather similarly, the induced RE action in the F state is obtained as

$$\delta\mathcal{S}_{RE} = \sum_{\mathbf{k},\omega_n}\sum_{b,b'}\left[\psi_b^\dagger(\mathbf{k}, i\omega_n)\chi_{bb'}^{RE}(\mathbf{k}, i\omega_n)\psi_{b'}(\mathbf{k}, i\omega_n) + \text{H.c.}\right], \tag{C10}$$

where

$$\chi_{AA}^{RE}(\mathbf{k}, i\omega_n) = -\frac{iJ_K^2}{4}\frac{\omega_n(\omega_n^2 + |g(\mathbf{k})|^2 + \lambda^2)\sigma^z}{(\omega_n^2 + \lambda^2)^2 + |g(\mathbf{k})|^2\omega_n^2},$$

$$\chi_{AB}^{RE}(\mathbf{k}, i\omega_n) = \frac{iJ_K^2}{4}\frac{\lambda^2 g(\mathbf{k})\sigma^z}{(\omega_n^2 + \lambda^2)^2 + |g(\mathbf{k})|^2\omega_n^2},$$

$$\chi_{BA}^{RE}(\mathbf{k}, i\omega_n) = -\frac{iJ_K^2}{4}\frac{\lambda^2 g^*(\mathbf{k})\sigma^z}{(\omega_n^2 + \lambda^2)^2 + |g(\mathbf{k})|^2\omega_n^2},$$

$$\chi_{BB}^{RE}(\mathbf{k}, i\omega_n) = -\frac{iJ_K^2}{4}\frac{\omega_n(\omega_n^2 + |g(\mathbf{k})|^2 + \lambda^2)\sigma^z}{(\omega_n^2 + \lambda^2)^2 + |g(\mathbf{k})|^2\omega_n^2}. \tag{C11}$$

The above order parameters indicate the emergence of a nonlocal order, which is completely polarized along the z direction.

2. Staggered configuration

The procedure to calculate the induced SC and RE actions for the AF state follows the same steps described in the last subsection. The hybridization matrix in this case is

$$\mathcal{V}_{AF}^\dagger = \frac{iJ_K}{\sqrt{2}}\begin{pmatrix} 0 & 0 & 0 & 0 & 0 & 0 & 0 & 0 \\ 0 & 0 & 0 & 0 & 0 & 0 & 0 & 0 \\ 0 & -1 & 1 & 0 & 0 & 0 & 0 & 0 \\ 0 & 0 & 0 & 0 & 1 & 0 & 0 & 1 \end{pmatrix}. \tag{C12}$$

The self-energy in Eq. (C2) has the form

$$\Sigma_{AF}(\mathbf{k}, i\omega_n) = \Sigma_{AF}^N(\mathbf{k}, i\omega_n) + \Sigma_{AF}^{SC}(\mathbf{k}, i\omega_n) + \Sigma_{AF}^{RE}(\mathbf{k}, i\omega_n), \tag{C13}$$

where

$$\Sigma_{AF}^N(\mathbf{k}, i\omega_n) = \frac{J_K^2}{2}\mathbb{1}_4 \otimes i\Omega(\mathbf{k}, i\omega_n)$$

$$\Sigma_{AF}^{SC}(\mathbf{k}, i\omega_n) = \frac{J_K^2}{2}\begin{pmatrix} -i\Omega(\mathbf{k}, i\omega_n)(\rho^x\sigma^x + \rho^y\sigma^y) & \Gamma(\mathbf{k}, i\omega_n)(\rho^y + i\rho^x\sigma^z) \\ \Gamma^*(\mathbf{k}, i\omega_n)(\rho^y - i\rho^x\sigma^z) & i\Omega(\mathbf{k}, i\omega_n)(\rho^x\sigma^x + \rho^y\sigma^y) \end{pmatrix},$$

$$\Sigma_{AF}^{RE}(\mathbf{k}, i\omega_n) = \frac{J_K^2}{2}\begin{pmatrix} -i\Omega(\mathbf{k}, i\omega_n)\rho^z\sigma^z & -\Gamma(\mathbf{k}, i\omega_n)(\sigma^y + i\rho^z\sigma^x) \\ -\Gamma^*(\mathbf{k}, i\omega_n)(\sigma^y - i\rho^z\sigma^x) & i\Omega(\mathbf{k}, i\omega_n)\rho^z\sigma^z \end{pmatrix}. \tag{C14}$$

These results allow us to write down the induced SC action and the pairing functions shown in Eqs. (42) and (43).

Lastly, the RE action for the AF state is given by

$$\delta\tilde{\mathcal{S}}_{RE} = \sum_{\mathbf{k},\omega_n}\sum_{b,b'}\left[\psi_b^\dagger(\mathbf{k}, i\omega_n)\tilde{\chi}_{bb'}^{RE}(\mathbf{k}, i\omega_n)\psi_{b'}(\mathbf{k}, i\omega_n) + \text{H.c.}\right], \tag{C15}$$

where

$$\tilde{\chi}_{\mathrm{AA}}^{\mathrm{RE}}(\mathbf{k}, i\omega_n) = -\frac{iJ_K^2}{4} \frac{\omega_n(\omega_n^2 + |g(\mathbf{k})|^2 + \lambda^2)\sigma^z}{(\omega_n^2 + \lambda^2)^2 + |g(\mathbf{k})|^2\omega_n^2},$$

$$\tilde{\chi}_{\mathrm{AB}}^{\mathrm{RE}}(\mathbf{k}, i\omega_n) = \frac{iJ_K^2}{2} \frac{\lambda^2 g(\mathbf{k})\sigma^-}{(\omega_n^2 + \lambda^2)^2 + |g(\mathbf{k})|^2\omega_n^2},$$

$$\tilde{\chi}_{\mathrm{BA}}^{\mathrm{RE}}(\mathbf{k}, i\omega_n) = -\frac{iJ_K^2}{2} \frac{\lambda^2 g^*(\mathbf{k})\sigma^+}{(\omega_n^2 + \lambda^2)^2 + |g(\mathbf{k})|^2\omega_n^2},$$

$$\tilde{\chi}_{\mathrm{BB}}^{\mathrm{RE}}(\mathbf{k}, i\omega_n) = \frac{iJ_K^2}{4} \frac{\omega_n(\omega_n^2 + |g(\mathbf{k})|^2 + \lambda^2)\sigma^z}{(\omega_n^2 + \lambda^2)^2 + |g(\mathbf{k})|^2\omega_n^2}. \tag{C16}$$

As a result, the above order parameters contain polarization vectors which are no longer restricted to the z direction.

---

[1] P. Anderson, Resonating valence bonds: A new kind of insulator? Mater. Res. Bull. **8**, 153 (1973).

[2] P. W. Anderson, The resonating valence bond state in La$_2$CuO$_4$ and superconductivity, Science **235**, 1196 (1987).

[3] L. Savary and L. Balents, Quantum spin liquids: A review, Rep. Prog. Phys. **80**, 016502 (2016).

[4] L. Balents, Spin liquids in frustrated magnets, Nature (London) **464**, 199 (2010).

[5] X.-G. Wen, Topological orders and edge excitations in fractional quantum Hall states, Adv. Phys. **44**, 405 (1995).

[6] X.-G. Wen, Quantum orders and symmetric spin liquids, Phys. Rev. B **65**, 165113 (2002).

[7] A. Kitaev, Anyons in an exactly solved model and beyond, Ann. Phys. (NY) **321**, 2 (2006).

[8] M. Hermanns, I. Kimchi, and J. Knolle, Physics of the Kitaev model: Fractionalization, dynamic correlations, and material connections, Annu. Rev. Condens. Matter Phys. **9**, 17 (2018).

[9] S. M. Winter, A. A. Tsirlin, M. Daghofer, J. van den Brink, Y. Singh, P. Gegenwart, and R. Valentí, Models and materials for generalized Kitaev magnetism, J. Phys.: Condens. Matter **29**, 493002 (2017).

[10] H. Takagi, T. Takayama, G. Jackeli, G. Khaliullin, and S. E. Nagler, Concept and realization of Kitaev quantum spin liquids, Nat. Rev. Phys. **1**, 264 (2019).

[11] G. Khaliullin, Orbital order and fluctuations in mott insulators, Prog. Theor. Phys. Suppl. **160**, 155 (2005).

[12] G. Jackeli and G. Khaliullin, Mott Insulators in the Strong Spin-Orbit Coupling Limit: From Heisenberg to a Quantum Compass and Kitaev Models, Phys. Rev. Lett. **102**, 017205 (2009).

[13] J. G. Rau, E. K.-H. Lee, and H.-Y. Kee, Generic Spin Model for the Honeycomb Iridates Beyond the Kitaev Limit, Phys. Rev. Lett. **112**, 077204 (2014).

[14] J. S. Gordon, A. Catuneanu, E. S. Sorensen, and H.-Y. Kee, Theory of the field-revealed Kitaev spin liquid, Nat. Commun. **10**, 2041 (2019).

[15] G. Chen, R. Pereira, and L. Balents, Exotic phases induced by strong spin-orbit coupling in ordered double perovskites, Phys. Rev. B **82**, 174440 (2010).

[16] W. M. H. Natori, E. C. Andrade, E. Miranda, and R. G. Pereira, Chiral Spin-Orbital Liquids with Nodal Lines, Phys. Rev. Lett. **117**, 017204 (2016).

[17] W. M. H. Natori, M. Daghofer, and R. G. Pereira, Dynamics of a $j = \frac{3}{2}$ quantum spin liquid, Phys. Rev. B **96**, 125109 (2017).

[18] J. Romhányi, L. Balents, and G. Jackeli, Spin-Orbit Dimers and Noncollinear Phases in d^1 Cubic Double Perovskites, Phys. Rev. Lett. **118**, 217202 (2017).

[19] F. Wang and A. Vishwanath, Z_2 spin-orbital liquid state in the square lattice Kugel-Khomskii model, Phys. Rev. B **80**, 064413 (2009).

[20] W. Witczak-Krempa, G. Chen, Y. B. Kim, and L. Balents, Correlated quantum phenomena in the strong spin-orbit regime, Annu. Rev. Condens. Matter Phys. **5**, 57 (2014).

[21] W. M. H. Natori, E. C. Andrade, and R. G. Pereira, SU(4)-symmetric spin-orbital liquids on the hyperhoneycomb lattice, Phys. Rev. B **98**, 195113 (2018).

[22] M. G. Yamada, M. Oshikawa, and G. Jackeli, Emergent SU(4) Symmetry in $\alpha-$ZrCl$_3$ and Crystalline Spin-Orbital Liquids, Phys. Rev. Lett. **121**, 097201 (2018).

[23] H. Ishikawa, T. Takayama, R. K. Kremer, J. Nuss, R. Dinnebier, K. Kitagawa, K. Ishii, and H. Takagi, Ordering of hidden multipoles in spin-orbit entangled $5d^1$ Ta chlorides, Phys. Rev. B **100**, 045142 (2019).

[24] J. M. Baker, Interactions between ions with orbital angular momentum in insulators, Rep. Prog. Phys. **34**, 109 (1971).

[25] R. Shiina, H. Shiba, and P. Thalmeier, Magnetic-field effects on quadrupolar ordering in a Γ_8-quartet system CeB$_6$, J. Phys. Soc. Jpn. **66**, 1741 (1997).

[26] K. Kubo and T. Hotta, Multipole ordering in f-electron systems on the basis of a $j-j$ coupling scheme, Phys. Rev. B **72**, 144401 (2005).

[27] P. Santini, S. Carretta, G. Amoretti, R. Caciuffo, N. Magnani, and G. H. Lander, Multipolar interactions in f-electron systems: The paradigm of actinide dioxides, Rev. Mod. Phys. **81**, 807 (2009).

[28] S. B. Lee, S. Trebst, Y. B. Kim, and A. Paramekanti, Landau theory of multipolar orders in Pr$(Y)_2X_{20}$ Kondo materials $(Y = $Ti, V, Rh, Ir; $X = $Al, Zn), Phys. Rev. B **98**, 134447 (2018).

[29] F.-Y. Li, Y.-D. Li, Y. Yu, A. Paramekanti, and G. Chen, Kitaev materials beyond iridates: Order by quantum disorder and Weyl magnons in rare-earth double perovskites, Phys. Rev. B **95**, 085132 (2017).

[30] S.-H. Jang, R. Sano, Y. Kato, and Y. Motome, Antiferromagnetic Kitaev interaction in f-electron based honeycomb magnets, Phys. Rev. B **99**, 241106(R) (2019).

[31] J. Xing, E. Feng, Y. Liu, E. Emmanouilidou, C. Hu, J. Liu, D. Graf, A. P. Ramirez, G. Chen, H. Cao, and N. Ni, Néel-type antiferromagnetic order and magnetic field-temperature phase diagram in the spin-$\frac{1}{2}$ rare-earth honeycomb compound YbCl$_3$, Phys. Rev. B **102**, 014427 (2020).

[32] A. Koga, H. Tomishige, and J. Nasu, Ground-state and thermodynamic properties of an $S = 1$ Kitaev model, J. Phys. Soc. Jpn. **87**, 063703 (2018).

[33] J. Oitmaa, A. Koga, and R. R. P. Singh, Incipient and well-developed entropy plateaus in spin-S Kitaev models, Phys. Rev. B **98**, 214404 (2018).

[34] P. P. Stavropoulos, D. Pereira, and H.-Y. Kee, Microscopic Mechanism for a Higher-Spin Kitaev Model, Phys. Rev. Lett. **123**, 037203 (2019).

[35] X.-Y. Dong and D. N. Sheng, Spin-1 Kitaev-Heisenberg model on a two-dimensional honeycomb lattice, arXiv:1911.12854.

[36] C. Xu, J. Feng, M. Kawamura, Y. Yamaji, Y. Nahas, S. Prokhorenko, Y. Qi, H. Xiang, and L. Bellaiche, Possible Kitaev Quantum Spin Liquid State in 2D Materials with $S = 3/2$, Phys. Rev. Lett. **124**, 087205 (2020).

[37] C. Hickey, C. Berke, P. P. Stavropoulos, H.-Y. Kee, and S. Trebst, Field-driven gapless spin liquid in the spin-1 Kitaev honeycomb model, Phys. Rev. Research **2**, 023361 (2020).

[38] H. Yao, S.-C. Zhang, and S. A. Kivelson, Algebraic Spin Liquid in an Exactly Solvable Spin Model, Phys. Rev. Lett. **102**, 217202 (2009).

[39] C. Wu, D. Arovas, and H.-H. Hung, Γ-matrix generalization of the Kitaev model, Phys. Rev. B **79**, 134427 (2009).

[40] H. Yao and D.-H. Lee, Fermionic Magnons, Non-Abelian Spinons, and the Spin Quantum Hall Effect From an Exactly Solvable Spin-1/2 Kitaev Model with SU(2) Symmetry, Phys. Rev. Lett. **107**, 087205 (2011).

[41] V. Dwivedi, C. Hickey, T. Eschmann, and S. Trebst, Majorana corner modes in a second-order Kitaev spin liquid, Phys. Rev. B **98**, 054432 (2018).

[42] A. Abragam and B. Bleaney, *Electron Paramagnetic Resonance of Transition Ions*, International Series of Monographs on Physics (Oxford University Press, Oxford, 2012).

[43] U. F. P. Seifert, T. Meng, and M. Vojta, Fractionalized Fermi liquids and exotic superconductivity in the Kitaev-Kondo lattice, Phys. Rev. B **97**, 085118 (2018).

[44] W. Choi, P. W. Klein, A. Rosch, and Y. B. Kim, Topological superconductivity in the Kondo-Kitaev model, Phys. Rev. B **98**, 155123 (2018).

[45] S. Biswas, Y. Li, S. M. Winter, J. Knolle, and R. Valentí, Electronic Properties of $\alpha-$RuCl$_3$ in Proximity to Graphene, Phys. Rev. Lett. **123**, 237201 (2019).

[46] G. Zhang, J. S. Van Dyke, and R. Flint, Cubic hastatic order in the two-channel Kondo-Heisenberg model, Phys. Rev. B **98**, 235143 (2018).

[47] A. S. Patri, I. Khait, and Y. B. Kim, Emergent non-Fermi-liquid phenomena in multipolar quantum impurity systems, Phys. Rev. Research **2**, 013257 (2020).

[48] V. Berezinskii, New model of the anisotropic phase of superfluid ^{3}He, JETP Lett. **20**, 287 (1974).

[49] T. R. Kirkpatrick and D. Belitz, Disorder-Induced Triplet Superconductivity, Phys. Rev. Lett. **66**, 1533 (1991).

[50] A. Balatsky and E. Abrahams, New class of singlet superconductors which break the time reversal and parity, Phys. Rev. B **45**, 13125 (1992).

[51] P. Coleman, E. Miranda, and A. Tsvelik, Possible Realization of Odd-Frequency Pairing in Heavy Fermion Compounds, Phys. Rev. Lett. **70**, 2960 (1993).

[52] P. Coleman, E. Miranda, and A. Tsvelik, Odd-frequency pairing in the Kondo lattice, Phys. Rev. B **49**, 8955 (1994).

[53] D. Belitz and T. R. Kirkpatrick, Properties of spin-triplet, even-parity superconductors, Phys. Rev. B **60**, 3485 (1999).

[54] J. Linder and A. V. Balatsky, Odd-frequency superconductivity, Rev. Mod. Phys. **91**, 045005 (2019).

[55] Y. Tanaka, M. Sato, and N. Nagaosa, Symmetry and topology in superconductors – odd-frequency pairing and edge states, J. Phys. Soc. Jpn. **81**, 011013 (2012).

[56] P. M. R. Brydon, D. F. Agterberg, H. Menke, and C. Timm, Bogoliubov Fermi surfaces: General theory, magnetic order, and topology, Phys. Rev. B **98**, 224509 (2018).

[57] E. Colomés and M. Franz, Antichiral Edge States in a Modified Haldane Nanoribbon, Phys. Rev. Lett. **120**, 086603 (2018).

[58] Z. Nussinov and J. van den Brink, Compass models: Theory and physical motivations, Rev. Mod. Phys. **87**, 1 (2015).

[59] D. H. McMahon and R. H. Silsbee, Virtual phonon effects in the paramagnetic resonance of MgO:Fe^{++}, Phys. Rev. **135**, A91 (1964).

[60] G. Khaliullin and S. Okamoto, Quantum Behavior of Orbitals in Ferromagnetic Titanates: Novel Orderings and Excitations, Phys. Rev. Lett. **89**, 167201 (2002).

[61] E. H. Lieb, Flux Phase of the Half-Filled Band, Phys. Rev. Lett. **73**, 2158 (1994).

[62] V. P. Mineev and M. Sigrist, Basic theory of superconductivity in metals without inversion center, in *Non-Centrosymmetric Superconductors: Introduction and Overview*, edited by E. Bauer and M. Sigrist (Springer, Berlin, Heidelberg, 2012), pp. 129–154.

[63] S. Yip, Noncentrosymmetric superconductors, Annu. Rev. Condens. Matter Phys. **5**, 15 (2014).

[64] V. J. Emery and S. Kivelson, Mapping of the two-channel Kondo problem to a resonant-level model, Phys. Rev. B **46**, 10812 (1992).

[65] V. J. Emery and S. A. Kivelson, Solution of an Orbital Kondo Array, Phys. Rev. Lett. **71**, 3701 (1993).

[66] E. Abrahams, A. Balatsky, D. J. Scalapino, and J. R. Schrieffer, Properties of odd-gap superconductors, Phys. Rev. B **52**, 1271 (1995).

[67] O. Zachar, S. A. Kivelson, and V. J. Emery, Exact Results for a 1D Kondo Lattice from Bosonization, Phys. Rev. Lett. **77**, 1342 (1996).

[68] S. Hoshino, J. Otsuki, and Y. Kuramoto, Diagonal Composite Order in a Two-Channel Kondo Lattice, Phys. Rev. Lett. **107**, 247202 (2011).

[69] S. Hoshino, J. Otsuki, and Y. Kuramoto, Resolution of entropy $\ln \sqrt{2}$ by ordering in two-channel Kondo lattice, J. Phys. Soc. Jpn. **82**, 044707 (2013).

[70] P. Chandra, P. Coleman, and R. Flint, Hastatic order in the heavy-fermion compound URu$_2$Si$_2$, Nature (London) **493**, 621 (2013).

[71] J. S. Van Dyke, G. Zhang, and R. Flint, Field-induced ferrohastatic phase in cubic non-Kramers doublet systems, Phys. Rev. B **100**, 205122 (2019).

[72] R. M. Fernandes, P. P. Orth, and J. Schmalian, Intertwined vestigial order in quantum materials: Nematicity and beyond, Annu. Rev. Condens. Matter Phys. **10**, 133 (2019).

[73] O. Erten, P.-Y. Chang, P. Coleman, and A. M. Tsvelik, Skyrme Insulators: Insulators at the Brink of Superconductivity, Phys. Rev. Lett. **119**, 057603 (2017).

[74] T. H. Hsieh, H. Ishizuka, L. Balents, and T. L. Hughes, Bulk Topological Proximity Effect, Phys. Rev. Lett. **116**, 086802 (2016).

[75] T. H. Hsieh, Y.-M. Lu, and A. W. W. Ludwig, Topological bootstrap: Fractionalization from Kondo coupling, Sci. Adv. **3**, e1700729 (2017).

[76] J. A. Krieger, A. Pertsova, S. R. Giblin, M. Döbeli, T. Prokscha, C. W. Schneider, A. Suter, T. Hesjedal, A. V. Balatsky, and Z. Salman, Proximity-Induced Odd-Frequency Superconductivity in a Topological Insulator, Phys. Rev. Lett. **125**, 026802 (2020).

[77] Y. Cao, V. Fatemi, S. Fang, K. Watanabe, T. Taniguchi, E. Kaxiras, and P. Jarillo-Herrero, Unconventional superconductivity in magic-angle graphene superlattices, Nature (London) **556**, 43 (2018).

[78] H. C. Po, L. Zou, A. Vishwanath, and T. Senthil, Origin of Mott Insulating Behavior and Superconductivity in Twisted Bilayer Graphene, Phys. Rev. X **8**, 031089 (2018).

[79] K. S. Novoselov, A. Mishchenko, A. Carvalho, and A. H. Castro Neto, 2D materials and van der Waals heterostructures, Science **353**, aac9439 (2016).